Anomalous structure of $MgCO_3$ liquid and the buoyancy of carbonatite melts

Sean M. Hurt[a, b*] and Aaron S. Wolf[a]

*Corresponding author email address: seanhurt@umich.edu

[a] Department of Earth and Environmental Sciences, University of Michigan, 1100 N. University Ave., Room 2534, Ann Arbor, MI 48109, USA

[b] Division of Math and Science, Nation Park College, 101 College Dr., Hot Springs National Park, AR 71913, USA

[This preprint has been accepted for publication in the Earth and Planetary Science Letters]

Highlights

- The structure of $MgCO_3$ liquid is unique among the other alkaline earth carbonates.
- Mg^{2+} adopts anomalously low 4-fold coordination with O_2^- and CO_3^- anions.
- $MgCO_3$ dramatically lowers carbonate liquid density and increases compressibility.
- Assuming $MgCO_3$-like structure, Fe-rich carbonatites remain buoyant in the mantle

Abstract

$MgCO_3$ is one of the most important components of mantle-derived carbonatite melts, and yet also one of the most difficult to study experimentally. Attempts to constrain its thermodynamic properties are hampered by decarbonation, which occurs at only ~500 °C, far below its metastable 1 bar melting temperature. Molecular dynamic simulations, however, can predict the thermodynamic properties of the $MgCO_3$ liquid component in spite of experimental challenges. Using the recently developed empirical potential model for high-pressure alkaline-earth carbonate liquids (Hurt and Wolf 2018), we simulate melts in the $MgCO_3$-$CaCO_3$-$SrCO_3$-$BaCO_3$ system from 773 to 2373 K up to 20 GPa. At 1 bar, $MgCO_3$ liquid assumes a novel topology characterized by a 4-fold coordination of the metal cation (Mg) with both the carbonate molecule and oxygen ion; this is distinct from the other alkaline-earth carbonate liquids in which the metal cation is in ~6- and ~8-fold coordination with carbonate and oxygen. With increasing pressure, $MgCO_3$ liquid structure becomes progressively more like that of (Ca, Sr, Ba)CO_3 liquids with Mg^{2+} approaching 6-fold coordination with carbonate groups. The novel network topology of $MgCO_3$ liquid results in a melt that is significantly more buoyant and compressible than other alkaline-earth carbonate liquids. Simulations of mixed $MgCO_3$-bearing melts show that metal cation coordination with O

and C is independent of bulk composition. Mixed simulation also reveal that molar volume, compressibility, enthalpy and heat capacity do not mix ideally with (Ca, Sr, Ba)CO_3 liquids at 1 bar, a consequence of preferential metal-cation ordering in $MgCO_3$-bearing mixtures. As pressure increases, however, mixing progressively approaches ideality with respect to molar volume, becoming nearly ideal by 12 GPa. The model is further applied to mantle-derived primary carbonatite melts with compositions, temperatures and pressures determined by published phase equilibrium experiments. The voluminous structure of liquid $MgCO_3$ results in a buoyant melt that inhibits a density crossover with the surrounding mantle. Assuming $FeCO_3$ liquid also adopts the same anomalous high-volume structure as $MgCO_3$, we predict that even the most Fe-rich ferrocarbonatites would remain buoyant and be barred from sinking or stagnating in the mantle.

Keywords: $MgCO_3$ melt, carbonate liquid structure, carbonatite density, alkaline earth carbonates

1. Introduction

Carbonate plays an important role in partial melting of the mantle. It can lower the solidus of mantle peridotite and eclogite up to ~600 °C (e.g. Dasgupta and Hirschmann 2006; Hammouda 2003), producing low degree partial melts of 0.03-0.3% carbonatite liquid (e.g. Green and Wallace 1988; Dalton and Wood 1993; Dasgupta and Hirschmann 2006). Carbonatite liquids are highly mobile owing to their ultralow viscosities (e.g. Kono et al. 2014). They are efficient agents of metasomatism (e.g. Green and Wallace 1988), are important for the petrogenesis of ocean island basalts (e.g. Dasgupta et al. 2006) and impact the deep carbon cycle (e.g. Dasgupta and Hirschmann 2010).

Of all the carbonate liquid components, $MgCO_3$ is one of the most geologically relevant. Carbonate enters the mantle through subduction of hydrothermally altered oceanic crust (e.g. Staudigel et al. 1989). Calcium from $CaCO_3$ partitions readily into the silicate phases of the mantle and is replaced by Mg, establishing $MgCO_3$ as a dominant carbonate mantle component (Biellmann et al. 1993). Investigations into the composition of primary carbonatite melts produced by partial melting of carbonated mantle eclogite and peridotite show that $MgCO_3$ along with $CaCO_3$ and $FeCO_3$ are the major components of interest (Dalton and Wood 1993; Dalton and Presnall 1998; Hammouda 2003; Ghosh et al 2009).

Carbonated mantle systems have been extensively studied via phase equilibrium experiments (e.g. Dalton and Wood 1993; Dalton and Presnall 1998; Hammouda 2003; Ghosh et al 2009). While such experiments are immensely valuable, they have limitations. For example, small variations in the starting composition can result in marked changes to the location of the solidus in P-T space (Dasgupta and Hirschmann 2010). This is problematic given the significant compositional heterogeneity of carbonated mantle, both in its silicate and carbonate phases. Compositional complexity is further compounded by wide ranges of temperatures and pressures where partial melting may occur. Phase equilibrium experiments cannot be performed for every relevant composition, temperature and pressure. Furthermore, experimenters often adjust temperature and pressure together, making it difficult to disentangle temperature- and pressure-effects.

Thermodynamic models such as MELTS (Ghiorso et al. 2002) or THERMOCALC (Powell and Holland 1988) can help resolve these issues but they rely on knowledge of the standard state thermodynamic properties. For the most important carbonate crystal phases (e.g. magnesite, siderite and calcite), the standard state properties are well known (e.g. Berman et al. 1985). However, knowledge of the standard state thermodynamic properties of the respective liquids is limited because alkaline-earth carbonates and $FeCO_3$ decompose at temperatures lower than their 1 bar melting temperatures. In spite of the difficulties posed by decarbonation, some properties of the $CaCO_3$ liquid component have been determined experimentally such as 1 bar density and thermal expansion (e.g. Liu and Lange 2003; Hurt and Lange 2018) and 1 bar compressibility (O'Leary et al 2015; Hurt 2018). Some $CaCO_3$ liquid properties have also been determined at high pressure, such as the fusion curve (e.g. Li et al. 2017) and the high-pressure density and compressibility (Hudspeth et al. 2018). However, there is a notable absence of accurate determinations of the standard state thermodynamic properties of $MgCO_3$ and $FeCO_3$ liquid. This is due to the very low 1 bar decarbonation temperatures (only 500° C for $MgCO_3$, Hurst 1991), which makes experiments on $MgCO_3$- and $FeCO_3$-bearing liquids nearly impossible at 1 bar.

At present, MD simulations provide the only plausible path for obtaining the complete set of carbonate liquid endmember properties needed to incorporate carbonate-silicate melting into a thermodynamic modeling framework like MELTS. The empirical potential model presented in Hurt and Wolf (2018) is designed specifically for simulations of alkaline-earth carbonate liquids at mantle conditions. In this study, we apply that model to simulate liquids in the $MgCO_3$-$CaCO_3$-

$SrCO_3$-$BaCO_3$ quaternary system from 773 to 2373 K up to 20 GPa. The simulations supply crucial constraints on the standard state thermodynamic properties of $MgCO_3$ liquid which are difficult or impossible to determine experimentally. Apart from endmember thermodynamic properties, the simulations also explore liquid structure and mixing behavior in the $MgCO_3$-$CaCO_3$-$SrCO_3$-$BaCO_3$ quaternary system.

To assess whether carbonate melts are buoyant throughout the upper mantle and transition zone, simulations are also performed on $CaCO_3$-$MgCO_3$ binary compositions from 1.5 to 20 GPa and 1423 to 1873 K along various pressure-temperature paths approximating that of subducting slabs. The simulation composition, temperature and pressure are representative of near-solidus carbonatite melts formed by low-degree partial melting of carbonated eclogite and peridotite. This is done in order to estimate the density of primary carbonatite melts as a function of depth and determine whether any compositions of carbonate melt are sufficiently dense to either stagnate upon initial melting or sink into the lower mantle. Given the likely similarity of $MgCO_3$ and $FeCO_3$ liquid structures and volumes, we also explore the implications for ferrocarbonatite melts in the mantle.

2. Methods

For this study, we use a previously published empirical potential model for the simulation of alkaline-earth carbonate liquids using rigid ions and partial charges. A complete description of this model is available in (Hurt and Wolf 2018) where it was applied to the simulation of liquids in the $CaCO_3$-$SrCO_3$-$BaCO_3$ system. This model is now applied to molecular dynamic (MD) simulations of $MgCO_3$-bearing liquids performed using the LAMMPS code (Plimpton, 1995).

While we use an empirical potential model, first-principles MD (FPMD) studies have made many significant contributions to the study of magmatic melts in recent years, including carbonated-silicate systems (e.g. Gosh et al. 2017; Solomatova et al. 2019). Though FPMD is generally considered to provide more accurate estimates of interatomic forces than the empirical potential approach, FPMD simulations suffer from issues related to convergence, affecting the overall quality of simulated physical properties (e.g. Ganster et al. 2007). Empirical potential MD, when using well-trained potentials, can achieve results that are just as accurate as FPMD for bulk properties but at lower computational expense.

42 different liquid compositions are simulated within the $MgCO_3$-$CaCO_3$-$SrCO_3$-$BaCO_3$ quaternary over a temperature range of 773-2373 K and up to 20 GPa. These simulations extend

to such low temperatures—well below the crystallization point for pure endmembers—because these carbonate liquids can be stable as important components within mixed composition liquids, which remain molten at much lower temperatures. MD simulations are performed with a timestep of 1 fs and total runtimes of 120 ps. Each simulation begins with an equilibration phase of 60 ps using the canonical (NVE) ensemble with the Berendsen barostat and thermostat (Berendsen et al., 1984), which equilibrates quickly and smoothly but deviates slightly from the canonical ensemble. A second equilibration phase of 40 ps is performed under the NPT ensemble using the Nosé-Hoover barostats and thermostats (Nosé, 1984; Hoover, 1985). A third phase of 20 ps continues the NPT ensemble and constitutes the final production run.

Every simulation is checked to ensure that system energies and volumes have converged to within 0.02% and 0.27%, respectively. This level of volume convergence is achieved with a simulation size of 6860 atoms. All simulations are initialized with atomic positions and velocities corresponding to $CaCO_3$ liquid at 2.275 g/cm^3 density (equivalent to 1 bar pressure) and 1623 K.

3. Results

3.1 Equation of state of $MgCO_3$ liquid

Hurt and Wolf (2018) previously showed that $CaCO_3$, $SrCO_3$ and $BaCO_3$ liquids have remarkably similar properties, with nearly parallel compression curves, 1 bar molar volumes that increase systematically with cation radius and congruent thermal expansions. Such systematic variation in molar volume and congruent thermal expansions are corroborated by the experiments of Hurt and Lange (2019) and Hurt (2018). Simulated compression curves for (Ca, Sr, Ba)CO_3 liquids are shown in Fig. 1 (solid lines), together with a hypothetical curve representing the expected behavior for $MgCO_3$ liquid (dotted line) assuming it follows the systematic trend of the other alkaline-earth carbonates.

To investigate whether $MgCO_3$ liquid follows the trends observed among $CaCO_3$, $SrCO_3$ and $BaCO_3$, its thermodynamic properties of $MgCO_3$ have been calculated from MD simulations (complete details and results are listed in Table A.1). Following Hurt and Wolf (2018), we attempt to fit the $MgCO_3$ simulation results with a temperature-dependent 3rd order Birch-Murnaghan equation of state (EOS), but the resulting models show a markedly poor fit to the data, reflected in both large pressure residuals and large error bars on the fitted parameters (Table 1). Unlike (Ca, Sr, Ba)CO_3 liquids, $MgCO_3$ liquid is highly compressible at pressures <2 GPa and its rapid change

in molar volume cannot be accommodated by a 3rd order Birch-Murnaghan, thus requiring us to adopt a 4th order Birch-Murnaghan EOS (details of the EOS are available in Appendix A).

The full set of parameters for this EOS is given in Table 1. This 4th order Birch-Murnaghan EOS model recovers the simulated molar volumes in the 1100 – 2000 K temperature range up to 20 GPa with RMS volume residuals of 0.27 cm^3/mol (0.81%). The 1100 K compression curve predicted by this best-fit EOS model is shown in Fig. 1 along with the raw simulated molar volume data as a function of pressure up to 12 GPa. Our simulation results predict radically different compression behavior for $MgCO_3$ as compared to the expected compression curve based on the other three alkaline-earth carbonate components. The 1 bar molar volume is near that of $SrCO_3$ and decreases dramatically with pressure, implying a 1 bar compressibility far-exceeding that of the other alkaline-earth carbonate liquids. The compression curve rapidly flattens out and begins to parallel the other alkaline-earth carbonates at pressures > 5 GPa. The thermophysical properties of liquids derive from their average atomic structure, and thus we explore the pressure-dependent atomic structure of $MgCO_3$ liquid to discover the root cause for this unique behavior among the alkaline-earth carbonates.

3.2 Distinct structure of $MgCO_3$ liquid

Though liquids lack long-range order, they do possess short-range order that can be described using a pair distribution function (pdf). For a particular pair of atomic types (i and j), pdf curves give the average density of j atoms as a function of distance from atom i. Liquid structure can also be described by coordination numbers for a given atomic pair. Average coordination numbers are calculated as weighted averages of the pdf curves, $g_{ij}(r)$:

$$CN_{ij} = 4\pi \int_0^{r_1} r^2 g_{ij}(r) \rho_j \, dr \qquad \text{Eq. 1}$$

where r is the atomic separation distance, ρ_j is the average atomic number density of atom j, and r_1 is the maximum cutoff radius located at the first minimum in the PDF, representing the outer boundary of the first nearest-neighbor peak.

Hurt and Wolf (2018) used the same empirical potential model to simulate (Ca, Sr, Ba)CO_3 liquids, and demonstrated that they have remarkably similar liquid structures and coordination numbers for the metal-oxygen (M-O), carbon-carbon (C-C) and metal-carbon (M-C) pairs. At ambient pressure, C-C and M-C coordination numbers are the same for each liquid at 10.9 and 5.9

182 respectively. M-O coordination numbers are similar for the three endmember liquids, increasing
183 systematically from Ca to Ba (Ca-O: 6.9, Sr-O: 7.3 and Ba-O: 7.7).

184 Based on the new simulations performed in this study, we analyze the structure of $MgCO_3$
185 liquid. The 1 bar results are summarized in Fig. 2, which shows a distinctly different atomic
186 structure and coordination environment for $MgCO_3$ as compared to the other alkaline-earth
187 carbonate liquids, visible in terms of C-C, M-O and M-C pairs. See Appendix C and Fig. C.3 for
188 the detailed coordination distributions of all alkaline-earth liquids across a range of P-T conditions.
189 At 1 bar and 1100 K, the Mg-O and Mg-C coordination is fourfold. The average value of 4.0 is
190 distributed with 43% of Mg-O pairs in 4-fold coordination while 17% and 27% are in 3- and 5-
191 fold coordination (the remaining pairs are divided among 2- and 6-fold). C-C coordination (11.6)
192 is nearly ideal closest-packing, similar to $CaCO_3$-$SrCO_3$-$BaCO_3$ liquids which adopt slightly lower
193 values (10.6-11.3). The most significant and systematic difference for the alkaline-earth carbonates
194 is seen in the M-C pairs. The average CN for M-C pairs is between 5.8 and 6.1 for the other
195 alkaline-earth carbonate liquids, but is only 4.0 for $MgCO_3$—the same as in alkali carbonates (e.g.
196 Roest et al 2017). These differences are also mirrored in the coordination distributions, which show
197 a dramatically narrower range of values for $MgCO_3$ compared to the other alkaline-earth
198 carbonates. The standard deviation (average width) of the CN distribution for $MgCO_3$ at 1 bar is
199 0.46, nearly half that of the remaining alkaline-earth carbonates, which all show a width of 0.90
200 (Fig. C.3 in the Appendix).

201 To determine whether the unique structure of $MgCO_3$ liquid persists at high pressure,
202 isothermal compression simulations are analyzed at 1100 K between 1 bar and 12 GPa. M-C and
203 M-O coordination numbers are calculated at each pressure and shown in Fig. 3. As pressure
204 increases, the average Mg-O coordination number increases linearly from 4 (at 1 bar) to 5.6 (at 12
205 GPa). In the high-pressure regime, M-O coordination number adopts systematic behavior among
206 the alkaline-earth carbonates: the average coordination number is ~10 for Ba-O, ~9 for Sr-O, ~8
207 for Ca-O and ~6 for Mg-O. Thus, at pressure, the Mg-O coordination number is consistent with
208 what might be expected from periodic systematics. For the M-C coordination numbers, $CaCO_3$-
209 $SrCO_3$-$BaCO_3$ liquids average around 6 at 1 bar and then increase modestly to ~6.8 by 12 GPa.
210 For $MgCO_3$, the Mg-C coordination starts off at 4.0 at 1 bar and converges rapidly to values
211 consistent with the other alkaline-earth carbonates (~6). While the average 1 bar coordination of
212 the typical alkaline-earth carbonate liquids is 6.0, not a single Mg-C pair is in 6-fold coordination

within $MgCO_3$; by 5 GPa, ~30% of the Mg-C pairs are 6-fold coordinated. Simulations thus indicate that the liquid structure of $MgCO_3$ becomes progressively more like that of the other alkaline-earth carbonates with compression, becoming nearly indistinguishable by 12 GPa.

3.3 Non-ideal mixing for $MgCO_3$ liquid at low pressure

Hurt and Wolf (2018) simulated alkaline-earth carbonate liquids in three binary systems: $CaCO_3$-$SrCO_3$, $CaCO_3$-$BaCO_3$ and $SrCO_3$-$BaCO_3$. It was found that molar volumes and molar isobaric heat capacities and compressibility all mix ideally across a wide range of temperatures and pressures. To test whether such ideal mixing behavior extends to $MgCO_3$-bearing liquids, simulations of mixed liquids are performed in the $MgCO_3$-$CaCO_3$-$SrCO_3$-$BaCO_3$ quaternary system at 1 bar and 1100 K. For any property of interest, we define the mixing quantity as the deviation from a compositionally-weighted average of the endmembers:

$$\Delta Z_{mix} = Z - \sum Z_i X_i \qquad \text{Eq. 2}$$

where Z is the molar quantity of interest (like volume or enthalpy) for the liquid mixture, X_i is mol fraction of each endmember, and Z_i is the quantity for each pure endmember at the specified temperature and pressure. The ideality of mixing in terms of both volume and enthalpy is assessed for simulated Mg-carbonate binaries and visualized in Fig. 4 (with direct simulation results reported in Appendix Table C.2).

Properties determined from MD simulations always contain uncertainties due to random fluctuations and system size limitations. We can reduce the effects of this noise and better characterize non-ideal mixing by fitting a simple sub-regular mixing model to the simulated ΔV_{mix} and ΔH_{mix} values:

$$\Delta Z_{mix} = \left(w + \Delta w \left[X - \frac{1}{2}\right]\right) \cdot X[1 - X] \qquad \text{Eq. 3}$$

where ΔZ_{mix} is the mixing property for either volume or enthalpy, X is mol fraction of $MgCO_3$, and w and Δw are constants which have been fitted using least squares minimization. The best-fit values of w and Δw at 1100 K and 1 bar for all three binaries are given in Appendix Table C.3. Fig. 4 depicts ΔV_{mix} in panel a and ΔH_{mix} in panel b for each simulated mixture as a function of $MgCO_3$ content along with the best-fit sub-regular solution model (Eq. 3). Fig. 4a shows significant non-ideal volume of mixing for all binaries, especially along the $CaCO_3$-$MgCO_3$ binary

where ΔV_{mix} is as large as -0.87 ± .11 cm^3/mol. Volumes of mixing are nearly all predicted to be negative. For all binaries, the mixing behavior is slightly asymmetric; the magnitude of ΔV_{mix} reaches a maximum at 60-75 mol % $MgCO_3$. The non-ideal mixing of volumes in $MgCO_3$-bearing liquids means that volumetric derivative properties such as compressibility also cannot mix ideally.

The case of enthalpy of mixing (ΔH_{mix}) is closely analogous. Unlike liquids in the $CaCO_3$-$SrCO_3$-$BaCO_3$ system, enthalpy does not mix ideally among $MgCO_3$-bearing mixtures. Fig. 4b shows that ΔH_{mix} is uniformly negative or statistically consistent with zero across the binary for every mixture. The peak magnitude of ΔH_{mix} increases systematically from $CaCO_3$ (31 KJ/mol) to $BaCO_3$ (~12 KJ/mol). Within each binary, the magnitude of ΔH_{mix} peaks at 60-75 mol% $MgCO_3$. Interestingly, the $BaCO_3$-$MgCO_3$ system exhibits the lowest ΔV_{mix} but the highest ΔH_{mix}; this suggests that the mechanism responsible for non-ideal mixing in volumetric properties is not the same as the one driving non-ideal mixing in enthalpic properties.

Hurt and Wolf (2018) found that simulations predict isobaric heat capacities to mix ideally according to mol fraction in $CaCO_3$-$SrCO_3$-$BaCO_3$ liquids. Simulations in this study of $MgCO_3$-bearing binary liquids from 1100 to 2000 K enabled calculation of the isobaric 1 bar heat capacity. For $CaMg(CO_3)_2$, $SrMg(CO_3)_2$ and $BaMg(CO_3)_2$, the heat capacity is estimated to be 146, 140 and 139 J/mol, which are lower than their ideal values by 7%, 11%, and 9%, respectively. Heat capacities are thus systematically lower (9% on average) than expected for $MgCO_3$-bearing-systems.

3.4 Ideal mixing of $MgCO_3$ liquid at high pressure

Though its structure and compressive properties are distinct at low pressures, $MgCO_3$ liquid increasingly resembles other alkaline-earth carbonates at higher pressures. This is apparent in the compression curves, which become nearly parallel between 5 and 10 GPa as shown in Fig. 1. To further investigate, binary mixture simulations of $CaMg(CO_3)_2$, $SrMg(CO_3)_2$ and $BaMg(CO_3)_2$ are also performed at 1100 K up to 12 GPa, assessing whether volumes and enthalpies mix ideally at pressure. The values of ΔV_{mix} calculated from the resulting simulations are -0.02 ± .03, -0.13 ± .03 and -0.11 ± .03 cm^3/mol for $CaMg(CO_3)_2$, $SrMg(CO_3)_2$ and $BaMg(CO_3)_2$ respectively. These ΔV_{mix} values are dramatically smaller than at 1 bar (which range between -0.34 and -0.91 cm^3/mol). Fig. 5 shows the compression behavior of ΔV_{mix} at 1100 K, normalized to the pressure-dependent absolute volume difference between $CaCO_3$ and $MgCO_3$ liquid, $\Delta V_{MgCO3\text{-}CaCO3}$. This pressure-

dependent normalization is necessary since the molar volume of the $MgCO_3$-$CaCO_3$ binary mixture falls between the volumes of the pure endmembers, and thus at pressures where pure $CaCO_3$ and $MgCO_3$ volumes converge, ΔV_{mix} will appear small; normalizing to the volume difference between the endmembers corrects for this. As seen in the figure, ΔV_{mix} approaches 0 as pressure increases, reflecting increasingly ideal mixing.

At low pressures, metal-cation ordering provides a mechanistic explanation for non-ideal mixing of at least some of the properties in $MgCO_3$-bearing liquids (see Appendix C for a full discussion). Since ΔV_{mix} diminishes to nearly 0 at 12 GPa, we might expect to see little difference between Mg-Mg pdf curves in pure $MgCO_3$ versus $MgCO_3$ mixtures at that pressure. The inset on Figure 5 shows, in fact, that the structural difference between pure and mixed $MgCO_3$ liquids progressively lessens with pressure (up to 12 GPa), supporting the notion that metal cation ordering correctly explains non-ideal mixing in volumetric properties among $MgCO_3$-bearing liquids.

In contrast, the simulations indicate that non-ideal mixing of enthalpy does not disappear at high pressure like ΔV_{mix}. At 12 GPa, ΔH_{mix} for $CaMg(CO_3)_2$, $SrMg(CO_3)_2$ and $BaMg(CO_3)_2$ is calculated to be -2.9, -8.2 and -11.7 kJ/mol respectively. Normalizing ΔH_{mix} to the difference in enthalpy between the endmembers would yield a more meaningful comparison (since absolute values of enthalpy increase with pressure). This result gives a normalized ΔH_{mix} of -1.2%, -2.1% and -1.9% at 12 GPa compared to -1.1%, -1.8% and -4.5% at 1 bar for $CaMg(CO_3)_2$, $SrMg(CO_3)_2$ and $BaMg(CO_3)_2$, respectively. $BaMg(CO_3)_2$ is the only mixture that undergoes a significant reduction in ΔH_{mix} with pressure, while the normalized ΔH_{mix} for the other binary liquids remain unchanged. This suggests that cation ordering in $MgCO_3$-bearing liquids is not solely responsible for non-ideal mixing of enthalpies.

3.5 Mg coordination in $MgCO_3$-bearing liquid mixtures

In addition to analyzing bulk properties, we also explore the atomic structures of Mg-bearing mixtures across a wide range of compositions. One of the most important results that emerged from these multicomponent simulations is that Mg-O and Mg-C coordination is insensitive to bulk composition. This means that, Mg^{2+} retains its fourfold coordination with oxygen and carbonate even in mixtures, revealing how the structure and properties of pure $MgCO_3$ provide a window into the behavior of geologically-relevant melts. The full range of pdf curves for M-O, M-C and C-C pairs for all binary compositions are available in Appendix Fig. C.1. The

striking uniformity of pdf curves demonstrates how M-O, M-C and C-C pairs in binary liquids retain the same structure and coordination as in the pure liquids. Similarly, if small amounts of $CaCO_3$, $SrCO_3$ and $BaCO_3$ are mixed into $MgCO_3$ liquid, Ca^{2+}, Sr^{2+} and Ba^{2+} ions maintain their octahedral coordination with carbonate.

This is an important results because the anomalous properties of $MgCO_3$ liquid are most pronounced at low pressure where pure $MgCO_3$ does not melt congruently. While pure $MgCO_3$ liquid is not stable at 1 bar, it is stable as a component in a mixed liquid, for example, $K_2Mg(CO_3)_2$ (Sharma and Simons 1980). Our simulations show that, while mixing between $MgCO_3$ and the other alkaline-earth carbonates is not perfectly ideal, it is sufficiently close to yield useful estimates of its partial molar properties based on its pure-liquid properties.

4. Discussion

4.1 Fourfold cation coordination in $MgCO_3$ liquid at 1 bar

Previous molecular dynamic studies have found that most alkaline-earth carbonate liquids ($CaCO_3$, $SrCO_3$, $BaCO_3$) adopt similar 1 bar atomic structures, with metal cations in octahedral coordination with carbonate anions and 7-8 fold coordination with oxygen (e.g. Hurt 2018, Vuilleumier 2014). A thorough search of the literature reveals, to the best of our knowledge, that this study is the first to demonstrate that $MgCO_3$-bearing melts are unique among those of the alkaline-earth carbonates, with Mg in an average fourfold coordination with both oxygen and carbonate anions. This structural anomaly is all the more surprising, given that Mg-bearing carbonate crystals (magnesite, dolomite, huntite, and northsite) all possess 6-fold oxygen coordination.

In silicate crystals, Mg is also mostly in 6-fold coordination with oxygen, the only exceptions being spinel and åkermanite ($Ca_2Mg[Si_2O_7]$) which host Mg in fourfold coordination with O (e.g. Kroecker and Stebbins 2000). While Mg is mostly found in 6-fold coordination with O in solid silicate phases, it is possible for it to enter near 4-fold coordination upon melting, opening the door for similar behavior in carbonate systems. A good example of this behavior can be found in the crystal enstatite (Mg_2SiO_6), where Mg-O coordination is 6-fold but decreases to 4.35 in the liquid (Cormier and Cuello 2013).

In silicate melts and glasses, Mg rarely possesses such low average coordination numbers with oxygen as we've observed in our simulations. However, Mg-O coordination numbers of <5

329 have been observed across a wide range of compositions in silicate melts and glasses (e.g. Roy
330 1950; Waseda and Toguri 1977; Kubicki et al 1992; Shimodo et al 2008; Trcera et al 2009;
331 Cormier and Cuello 2013). Karki et al. (2018) performed FPMD simulations of silicate melts
332 with compositions representing mid-ocean ridge basalt and found an average Mg-O coordination
333 of 4.62; Guillot and Sator similarly performed classical MD simulations on systems analogous to
334 peridotite and found and average Mg-O coordination of 4.8. It should be noted that, while
335 common, Mg does not always assume such a low coordination state in all silicate melts and
336 glasses. For example, at 1 bar, Morizet et al. (2019) found an average Mg-O coordination of 5- to
337 6-fold from X-ray and neutron diffraction experiments on CO_2-bearing silicate glasses.
338 The average Mg-O coordination in carbonate melts is unfortunately difficult to assess from
339 past analytical studies. Detailed structural information on Mg^{2+} coordination in $MgCO_3$-bearing
340 carbonate melts/glasses is largely unavailable. This is in part because melt structure is commonly
341 determined via experimental analyses of glasses (such as XANES or EXAF), and while silicate
342 melts readily quench to glass, there is only one purely carbonate system that is capable of
343 vitrification: K_2CO_3-$MgCO_3$ (e.g. Datta et al 1964; Ragone et al 1966). This system is doubly
344 unique because it is the only known $MgCO_3$-bearing carbonate liquid that forms a stable melt at 1
345 bar (Ragone et al 1966). K_2CO_3-$MgCO_3$ glass structures have been studied by both infrared (Datta
346 et al 1964; Genge et al 1995) and Raman spectroscopy (Sharma and Simons 1980; Genge et al
347 1995). Neither Genge nor Sharma comment on Mg^{2+} coordination in their spectroscopic studies.
348 However, Datta et al (1964) posited that the low refractive index and density of the K_2CO_3-$MgCO_3$
349 glass (compared to the respective crystals) may result from a low (4-fold) Mg coordination. Datta
350 also recognized the significance of the fact that the only known $MgCO_3$-bearing carbonate liquid
351 that is stable at 1 bar is also the only carbonate capable of quenching to a glass, implying its
352 structure must somehow be unique among alkaline-earth carbonate liquids; Datta thus
353 hypothesized that it could be related to a decrease in Mg^{2+} coordination number. Our MD
354 simulations suggest that $MgCO_3$ liquid does in fact assume a unique topology characterized by a
355 low (4-fold) coordination of Mg^{2+}, which corroborates the suppositions of Datta et al. (1964) on
356 the structure of $MgCO_3$-bearing carbonate melts.

357 ***4.2 Comparison of $MgCO_3$ to other alkaline-earth carbonate liquids***

358 From the simulations of this study, it appears that $MgCO_3$ has a liquid structure that is
359 distinct from the other alkaline-earth carbonates and properties that deviate strongly from those

predicted on the basis of systematic variations (see Hurt 2018; Hurt and Lange 2019). Hurt and Lange (2019) explored systematic variations in the 1 bar molar volumes of alkali and alkaline-earth carbonate liquids. On the basis of systematic trends, two different estimates of $MgCO_3$ liquid molar volume were made; one estimate assumes that the CN of Mg-C and Mg-O are both 6 and has a liquid structure that is like the other alkaline-earth carbonates. The other estimate assumes the CN of Mg-O and Mg-C is 4 and has a liquid structure that is more like an alkali carbonate. Under the 6-fold assumption, Hurt and Lange predict a 1 bar $MgCO_3$ liquid molar volume of 34.4 ± .6 cm^3/mol. In the case of a 4-fold Mg-O coordination, Hurt and Lange (2019) estimated that $MgCO_3$ would have a 1 bar liquid molar volume of ~40 cm^3/mol at 1100 K.

Our simulations clearly predict 4-fold coordination for Mg^{2+} and a liquid structure that is more like alkali carbonate than typical alkaline-earth carbonates (a full discussion of similarities between $MgCO_3$ and alkali carbonate liquid structure is available in Appendix B). In accordance with the estimates of Hurt and Lange (2019), our simulations predict a larger 1 bar molar volume than what might be expected from systematic variations in the molar volumes of alkaline-earth carbonate liquids. The fitted Birch-Murnaghan EOS model (Appendix Eq. A.1-A.4) predicts a 1 bar $MgCO_3$ liquid volume of 44.21±.09 cm^3/mol at 1100 K. However, it's likely that the actual volume is somewhat lower since the empirical potential model of Hurt and Wolf (2018) typically slightly overestimates 1 bar volumes. For $CaCO_3$, $SrCO_3$ and $BaCO_3$ liquids, the model requires a -0.35, -0.33 and -0.75 GPa pressure correction, respectively, to bring simulated 1 bar volumes into agreement with the experimental projections of Hurt and Lange (2019). An analogous -0.6 GPa pressure correction would bring the $MgCO_3$ simulations into agreement with the alkali-like structural predictions from Hurt and Lange (2019).

Hurt (2018), provides analogous systematic trend equations for the compressibility of alkali and alkaline-earth carbonate liquids based on a positive linear relationship between liquid compressibility and volume of fusion. Their model equation predicts a compressibility for $MgCO_3$ liquid at 1100 K of ~23±1 10^{-2} GPa^{-1}, assuming it fits into the alkali carbonate trend, and ~18±6 10^{-2} GPa^{-1} if it fits into the alkaline-earth trend. Given the similarity of the $MgCO_3$ liquid structure to Li_2CO_3 (Appendix Fig. B.1), the alkali carbonate trend might actually provide a better prediction (for more details regarding similarities between $MgCO_3$ and alkali carbonates, see Appendix B). These estimates of $MgCO_3$ liquid compressibility differ dramatically from other alkaline-earth carbonate liquids (i.e. $CaCO_3$, $SrCO_3$ and $BaCO_3$) which have relatively modest 1 bar/1100 K

compressibilities of 4.33 - 5.97 · 10^{-2} GPa^{-1}. Our $MgCO_3$ liquid simulations predict a bulk modulus (K_T) of 6.15±.15 GPa, which is equivalent to a compressibility (β_T) of 16.3 · 10^{-2} GPa^{-1} at 1100 K, broadly consistent with the elevated values predicted by Hurt (2018).

4.3 Comparison to previous thermodynamic studies of $MgCO_3$ liquid properties

As noted above, the structure of $MgCO_3$ liquid becomes more like the other alkaline-earth carbonates with greater pressure. By 12 GPa, the Mg-O and Mg-C coordination converge to values in line with $CaCO_3$, $SrCO_3$, and $BaCO_3$ liquids (Fig. 2). This pressure-induced transformation of liquid structure is also evident in the compression curve of $MgCO_3$ liquid, which begins to parallel the other three alkaline-earth carbonate liquids at 5-10 GPa (Fig. 1).

Our predictions of the standard state thermodynamic properties of $MgCO_3$ liquid stand in stark contrast to previous estimates made by Kang et al. 2016. These calculations fit a thermodynamic model to the congruent melting curve of $MgCO_3$, which is bracketed by four experimentally determined points (~1858 K at 3 GPa & 1883 K at 3.6 GPa from Irving and Wyllie 1975, and 2183 K at 8 GPa & 2363 K at 15 GPa from Katsura and Ito 1990). This approach arrives at a molar volume of $MgCO_3$ liquid of ~32 cm^3/mol and a compressibility of 2.6 · 10^{-2} GPa^{-1} at 1100 K and 1 bar. While the $MgCO_3$ properties proposed by Kang et al. differ markedly from our simulation results, Kang et al. arrived at their values using a method that is statistically problematic. The estimates of standard state thermodynamic properties of $MgCO_3$ liquid (and $FeCO_3$ as well) proposed by Kang et al. were calculated by fusion curve analysis. The fusion curve of $MgCO_3$ is currently bracketed by 4 experimental points (and only 3 for $FeCO_3$). However, 5 thermodynamic parameters are fitted to each dataset. Since the number of fitted parameters exceeds the number of constraining observations, the reported thermodynamic solution is highly under-constrained and non-unique, allowing alternative sets of thermodynamic properties to perfectly recover the limited observables.

We can see some of the resulting issues directly in the fitted thermodynamic properties proposed by Kang et al. (2016); for example, Kang gives thermal expansions of $MgCO_3$ and $FeCO_3$ liquid that are identical to the thermal expansion of their respective crystal phases. However, the thermal expansion of a liquid is generally expected to be substantially greater than that of the crystal (e.g. Lange 1997). $CaCO_3$, $SrCO_3$ and $BaCO_3$ liquids, for example, have thermal expansions ~3 times greater than their respective crystal phases (Hurt and Lange 2018). Kang et al. also give a temperature dependence of compressibility ($\delta\beta_T/\delta T$) of $MgCO_3$ liquid that is lower,

by an order of magnitude, than those of $CaCO_3$, $SrCO_3$ and $BaCO_3$ liquids (Hurt et al. 2018). For these reasons, we strongly recommend the standard state $MgCO_3$ liquid thermodynamic properties derived from this study.

4.4 The density of primary carbonatite melts

Natural carbonatite liquids have been shown to be effective agents of mantle metasomatism and scavengers of trace elements (e.g. Blundy and Dalton 2000), and thus the mobility and ascent rates of primary carbonatite melts are particularly important. Ascent rate depends mostly on melt viscosity and density contrast. Viscosity has been measured at temperatures and pressure representative of the mantle for calcitic and dolomitic liquids (e.g. Kono et al. 2014); and the density of $CaCO_3$ liquid has been determined experimentally at 1 bar (e.g. Hurt and Lange 2018) and at high-pressure (Hudspeth et al 2018). However, primary carbonatite melts generated in the mantle by low-degree partial melting contain significant amounts of $MgCO_3$ and $FeCO_3$ (e.g. Dalton and Wood 1993; Ghosh et al. 2009).

While the densities of primary carbonatite melts along a carbonated mantle liquidus are mostly unknown, it may be estimated by simulations from this study. Using the compositions of low-degree primary carbonatite melts generated in phase equilibrium experiments of carbonated peridotite and eclogite (Dalton and Wood 1993; Dalton and Presnall 1998; Hammouda 2003; Ghosh et al. 2009), simulations at temperature and pressure are performed for simplified experimental compositions by projecting them into the $CaCO_3$-$MgCO_3$ binary. Complete details on these calculations are available in Appendix D.

The simulated density results are listed in Table 2 and depicted as a function of depth in Fig. 6. The simulations indicate that $CaCO_3$-$MgCO_3$ binary liquids will be relatively low in density due to the open network topology of the $MgCO_3$ melt component. Thus, primary carbonatite melts maintain a significant density contrast with the surrounding mantle rocks throughout the entire upper mantle and transition zone. Even the densities of melts from Hammouda (2003), which represent a cold slab subduction PT path (and are relatively enriched in denser $CaCO_3$ and $FeCO_3$ components) never approach that of the mantle. Given the ultralow viscosity of these kinds of liquids, any positive density contrast will swiftly drive liquid ascent; any degree of carbonate melt will thus quickly escape from a descending slab, inhibiting the subduction and storage of carbonate into the lower mantle.

The only common carbonate component heavy enough to potentially affect a density crossover in the mantle is $FeCO_3$ (which is a common component in mantle-derived carbonatite melts, e.g. Hammouda 2003). Though our work does not directly address iron partitioning in carbonate-rich melts, we can use our model to approximate a minimum threshold iron-content that a hypothetical ferrocarbonatite must contain in order to affect a density crossover within the mantle. While $FeCO_3$ liquid was not directly simulated in this study, it's likely that $FeCO_3$ shares the volumetric properties of $MgCO_3$, since Fe^{2+} and Mg^{2+} have the same valence and similar ionic radii, and thus can frequently occupy the same atomic sites within crystal lattices and liquid pseudo-lattices. Assuming that $MgCO_3$ liquid molar volume is a reasonable proxy for $FeCO_3$, the $FeCO_3$ concentration necessary for affecting a density crossover can be calculated as a function of depth for a ferrocarbonatite in the $MgCO_3$-$CaCO_3$-$FeCO_3$ system. For the purposes of this calculation, it will be assumed that the molar volumes of all three components mix ideally and that $X^{Mg} = X^{Ca}$. The $MgCO_3$ & $FeCO_3$ liquid volumes are approximated at temperature and pressure using the thermodynamic properties presented this study (Table 1) in conjunction with Eqs. A.1-A.4.

The partial molar volume of the $CaCO_3$ liquid component is accurately estimated by combining experimental and theoretical constraints, using a 3rd order Birch-Murnaghan EOS with properties taken from the 1 bar molar volume model of Hurt and Lange (2019), the compressibility results of Hurt (2018) and the *K'* results from Hurt and Wolf (2018). The partial molar volume of the $MgCO_3$, $FeCO_3$ and $CaCO_3$ components were calculated at P-T conditions along an average carbonated peridotite solidus given by Dasgupta and Hirschmann (2010):

$$T(°C) = 0.0238 \times P^3 - 2.2084 \times P^2 \times 73.7991 \times P + 830.3808 \qquad \text{Eq. 4}$$

where P is in GPa. Using this approach, Fig. 7a shows the minimum requisite $FeCO_3$ concentration needed for a ferrocarbonatite to stagnate in the mantle gradually decreases through the upper mantle from a mol fraction of ~1 in the crust, to 0.5 (35 wt.% FeO) at the top of the transition zone. Throughout the transition zone, the threshold iron content is ~0.65 mol fraction $FeCO_3$. Such iron concentrations far exceed what's observed in phase equilibrium experiments on carbonated peridotite/eclogite (which generally produce carbonatite melts with <10 wt. % FeO). Fig. 7b shows the density of a melt with an approximate composition of a natural ferrocarbonatite (Thompson et

al. 2002) which was calculated as a function of depth using the technique described above. As evident, its density remains consistently lower than the mantle through the transition zone.

It's difficult to assess with certainty whether significant volumes of such highly Fe-enriched (>40 mol% $FeCO_3$) ferrocarbonatites are actually produced in the mantle. After an exhaustive search of the literature, the ferrocarbonatite in Swartbooisdrif, Namibia (Thompson et al. 2002) appears to be the only natural ferrocarbonatite yet identified with an unambiguously magmatic origin. Thompson gives its composition as approximately $Fe_{0.26}\ Mg_{0.22}\ Ca_{0.52}\ CO_3$. We find it interesting that the Swartbooisdrif ferrocarbonatite has a composition nearly identical to that of Ankerite, $Ca(Mg,Fe)(CO_3)_2$. If $FeCO_3$ behaves similarly to $MgCO_3$, we might expect an equilibrium liquid composition resulting from partial melting that is roughly equal parts Fe and Mg to be energetically favorable within the $FeCO_3$-$MgCO_3$-$CaCO_3$ ternary. Given the lack of natural samples, the energetic and volumetric properties predicted by our simulations, and the measured Fe-contents found in melting experiments on carbonated mantle materials, we find that ferrocarbonatites are unlikely to have sufficient Fe-enrichment to stagnate in the mantle owing to their large relative buoyancy.

5. Conclusions

We perform classical MD simulations of $MgCO_3$-bearing liquids using the empirical potential model of Hurt and Wolf (2018) at mantle pressures and temperatures. We find that $MgCO_3$ liquid assumes a novel topology characterized by four-fold coordination of Mg^{2+} with both the carbonate molecule and O^{2-}. Such a structure is markedly different from that of the other alkaline-earth carbonate liquids in which the metal cation is in 6-fold coordination with the carbonate molecule and 7-8 fold coordination with oxygen atoms. The liquid structure and resulting thermodynamic properties of $MgCO_3$ are found to be more similar to that of Li_2CO_3 than other alkaline-earth carbonate liquids, resulting in a dramatically more buoyant and compressible liquid than previous studies have suggested. The voluminous structure and subsequent low density of $MgCO_3$-rich liquids bolsters the density contrast of $MgCO_3$-bearing carbonatite melts in the mantle, increasing their already significant rates of ascent and preventing even relatively dense ferrocarbonatite melts from achieving a density crossover with the surrounding mantle.

The simulations have further suggested that $MgCO_3$ molar volume, thermal expansivity, compressibility, enthalpy and heat capacity do not mix ideally with (Ca, Sr, Ba)CO_3 liquids. Non-ideal mixing of volumetric properties stems from localized metal cation ordering around the Mg^{2+}

ion. We find that it is energetically favorable to surround tetrahedral Mg-CO_3 complexes with octahedral Ca-, Sr-, Ba-carbonate complexes. This effect gradually diminishes with pressure, where $MgCO_3$ molar volume is found to mix near-ideally with $CaCO_3$-$SrCO_3$-$BaCO_3$ liquids by 12 GPa. On the other hand, non-ideal mixing of enthalpy in $MgCO_3$-bearing systems persists even at high pressure.

The novel topology of $MgCO_3$ liquid indicated by our simulations opens questions on another important component in mantle-derived carbonatite melts: $FeCO_3$. Given the similar ionic radii of Fe^{2+} and Mg^{2+}, it's possible that Fe^{2+} also assumes a 4-fold coordination with $(CO_3)^{2-}$ and O^{2-} in $FeCO_3$ liquid, producing a similar liquid structure to $MgCO_3$; the result would be a $FeCO_3$ component that is significantly less dense than what has been expected by other studies (e.g. Kang and Schmidt 2016, 2017). Such a voluminous $FeCO_3$ component would inhibit ferrocarbonatite melts generated within subducting slabs from ever stagnating or sinking in the mantle, due to their low relative densities. Multi-angle energy dispersive X-ray diffraction experiments on $MgCO_3$- and $FeCO_3$-bearing melts are needed in order to verify the liquid structure of these important carbonate components.

Acknowledgements: The authors would like to acknowledge Becky Lange, Udo Becker, Youxue Zhang and Will Bender, as well as two anonymous reviewers, for their helpful comments throughout the development of the research. S.H and A.S.W. thank NSF-1763189 for primary financial support for this work, and S.H. also thanks the Rackham Merit Fellowship for additional financial support.

References

Berendsen H. J. C., Postma J. P. M., Van Gunsteren W. F., Di Nola A. and Haak J. R. (1984) Molecular dynamics with coupling to an external bath. *J. Chem. Phys.* **81**, 3684–3690.

Berman R. G. and Brown T. H. (1985) Heat capacity of minerals in the system Na_2O-K_2O-CaO-MgO-FeO-Fe_2O_3-Al_2O_3-SiO_2-TiO_2-H_2O-CO_2: representation, estimation, and high temperature extrapolation. *Contrib. to Mineral. Petrol.* **89**, 168–183.

Biellmann C., Gillet P., Guyot F., Peyronneau J. and Reynard B. (1993) Experimental evidence for carbonate stability in the Earth's lower mantle. *Earth Planet. Sci. Lett.* **118**, 31–41.

Blundy J. and Dalton J. (2000) Experimental comparison of trace element partitioning between clinopyroxene and melt in carbonate and silicate systems, and implications for mantle metasomatism. *Contrib. to Mineral. Petrol.* **139**, 356–371.

Cormier L. and Cuello G. J. (2013) Structural investigation of glasses along the $MgSiO_3$-$CaSiO_3$ join: Diffraction studies. *Geochim. Cosmochim. Acta* **122**, 498–510.

Dalton J. A. and Presnall D. C. (1998) Carbonatitic melts along the solidus of model lherzolite in the system CaO-MgO-Al_2O_3-SiO_2-CO_2 from 3 to 7 GPa. *Contrib. to Mineral. Petrol.* **131**, 123–135.

Dalton J. A. and Wood B. J. (1993) The compositions of primary carbonate melts and their evolution through wallrock reaction in the mantle. *Earth Planet. Sci. Lett.* **119**, 511–525.

Dasgupta R. and Hirschmann M. M. (2006) Melting in the Earth's deep upper mantle caused by carbon dioxide. *Nature* **440**, 659–662.

Dasgupta R. and Hirschmann M. M. (2010) The deep carbon cycle and melting in Earth's interior. *Earth Planet. Sci. Lett.* **298**, 1–13.

Datta R. K., Roy D. M., Faile S. P. and Tuttle O.F. (1964) Glass formation in carbonate systems. *J. Am. Ceram. Soc.* **47**, 153. https://doi.org/10.1111/j.1151-2916.1964.tb14377.x

557 Ganster P., Benoit M., Delaye J.M., Kob W. (2007) Structural and vibrational properties of a
558 calcium aluminosilicate glass: classical force-fields vs. first-principles. *Mol. Simul.* **33**, 1093–
559 1103.

560 Genge M. J., Price G. D. and Jones A.P. (1995) Molecular dynamics simulations of $CaCO_3$ melts
561 to mantle pressures and temperatures: implications for carbonatite magmas *Earth Planet. Sci.*
562 *Lett.* **131**, 225-238. *Sci. Rep.* **7**

563 Ghiorso M. S., Hirschmann M. M., Reiners P. W. and Kress V. C. (2002) The pMELTS: A revision
564 of MELTS for improved calculation of phase relations and major element partitioning related
565 to partial melting of the mantle to 3 GPa. *Geochemistry Geophys. Geosystems* **3**, 36.

566 Ghosh D.B., Bajgain S.K., Mookherjee M. and Karki B.B. (2017) Carbon-bearing silicate melt at
567 deep mantle conditions **7**, 848.

568 Ghosh S., Ohtani E., Litasov K. D. and Terasaki H. (2009) Solidus of carbonated peridotite from
569 10 to 20 GPa and origin of magnesiocarbonatite melt in the Earth's deep mantle. *Chem. Geol.*
570 **262**, 17–28.

571 Green D. H., Wallace M. E. (1988) Mantle metasomatism by ephemeral carbonatite melts. *Nature*
572 **336**, 459–462.

573 Guillot B. and Sator N. (2007) A computer simulation study of natural silicate melts. Part II: High
574 pressure properties. *Geochim. Cosmochim. Acta* **71** 4538-4556.

575 Hammouda T. (2003) High-pressure melting of carbonated eclogite and experimental constraints
576 on carbon recycling and storage in the mantle. *Earth Planet. Sci. Lett.* **214**, 357–368.

577 Hoover W. G. (1985) Canonical dynamics: Equilibrium phase-space distributions. *Phys. Rev. A*
578 **31**, 1695–1697.

579 Hudspeth J., Sanloup C. and Kono Y. (2018) The properties of molten $CaCO_3$ at high pressure.
580 *Geochem. Persp. Let.* **7**, 17-21.

581 Hurst H. J. (1991) The thermal decomposition of magnesite in nitrogen. *Thermochim. Acta* **189**,
582 91–96.

583 Hurt S.M. (2018) The thermodynamic properties and structure of alkali and alkaline earth
584 carbonate melts, Ph.D. thesis, University of Michigan, Ann Arbor.

585 Hurt S. M. and Lange R. A. (2019) The density of Li_2CO_3-Na_2CO_3-K_2CO_3-Rb_2CO_3-Cs_2CO_3-
586 $CaCO_3$-$SrCO_3$-$BaCO_3$ liquids: New measurements, ideal mixing, and systematic trends with
587 cation coordination. *Geochim. Cosmochim. Acta* **248**, 123–137.

588 Hurt S. M. and Wolf A. S. (2018) Thermodynamic properties of $CaCO_3$-$SrCO_3$-$BaCO_3$ liquids: a
589 molecular dynamics study using new empirical atomic potentials for alkaline earth
590 carbonates. *Phys. Chem. Miner.* https://doi-org.proxy.lib.umich.edu/10.1007/s00269-018-
591 0995-5

592 Irving A. J. and Wyllie P. J. (1975) Subsolidus and melting relationships for calcite, magnesite
593 and the join $CaCO_3$-$MgCO_3$ 36 kb. *Geochim. Cosmochim. Acta* **39**, 35–53.

594 Kang N. and Schmidt M. W. (2017) The melting of subducted banded iron formations. *Earth*
595 *Planet. Sci. Lett.* **476**, 165–178.

596 Kang N., Schmidt M. W., Poli S., Connolly J. A. D. and Franzolin E. (2016) Melting relations in
597 the system $FeCO_3$-$MgCO_3$ and thermodynamic modelling of Fe-Mg carbonate melts.
598 *Contrib. to Mineral. Petrol.* **171**, 1-16.

599 Karki B.B., Ghosh D.B., and Bajgain S.K. (2018) Simulation of silicate melts under pressure, in:
600 Kono, Y., Sanloup C. (Eds.), Magmas Under Pressure: Advances in High-Pressure
601 Experiments on Structure and Properties of Melts. Elsevier, Cambridge, pp. 419-453.

602 Katsura T. and Ito E. (1990) Melting and subsolidus phase relations in the $MgSiO_3$-$MgCO_3$ system
603 at high pressures: implications to evolution of the Earth's atmosphere. *Earth Planet. Sci. Lett.*
604 **99**, 110–117.

605 Kono Y., Kenney-Benson C., Hummer D., Ohfuji H., Park C., Shen G., Wang Y., Kavner A. and
606 Manning C. E. (2014) Ultralow viscosity of carbonate melts at high pressures. *Nat. Commun.*
607 **5**, 5091.

608 Kress V. C., Williams Q. and Carmichael I. S. E. (1988) Ultrasonic investigation of melts in the
609 system Na_2O-Al_2O_3-SiO_2. *Geochim. Cosmochim. Acta* **52**, 283–293.

610 Kroeker S. and Stebbins J. F. (2000) Magnesium coordination environments in glasses and
611 minerals: New insight from high-field magnesium-25 MAS NMR. *Am. Mineral.* **85**, 1459–
612 1464.

613 Kubicki J. D., Hemley R. J. and Hofmeister A. M. (1992) Raman and infrared study of pressure-
614 induced structural changes in $MgSiO_3$, $CaMgSi_2O_6$, and $CaSiO_3$ glass. *Am. Mineral.* **77**, 258-
615 262.

616 Lange R. A. (1997) A revised model for the density and thermal expansivity of K_2O-Na_2O-CaO-
617 MgO-Al_2O3-SiO_2 liquids from 700 to 1900 K: extension to crustal magmatic temperatures.
618 *Contrib. to Mineral. Petrol.* **130**, 1–11.

619 Liu Q. and Lange R. A. (2003) New density measurements on carbonate liquids and the partial
620 molar volume of the $CaCO_3$ component. *Contrib. to Mineral. Petrol.* **146**, 370–381.

621 Morizet Y., Trcera N., Larre C., Rivoal M., Le Menn E., Vantelon D. and Gaillard F. (2019) X-
622 ray absorption spectroscopic investigation of the Ca and Mg environments in CO_2-bearing
623 silicate glasses. *Chem. Geol.* **510**, 91-102.

624 Nosé S. (1984) A unified formulation of the constant temperature molecular dynamics methods.
625 *J. Chem. Phys.* **81**, 511.

626 O'Leary M. C., Lange R. A. and Ai Y. (2015) The compressibility of $CaCO_3$-Li_2CO_3-Na_2CO_3-
627 K_2CO_3 liquids: Application to natrocarbonatite and CO_2-bearing nephelinite liquids from
628 Oldoinyo Lengai. *Contrib. to Mineral. Petrol.* **170**, 1-18.

629 Plimpton S. (1995) Fast parallel algorithm for short-range molecular dynamics. *J. Comput.*
630 *Phys.***117,** 1-42.

631 Powell R. and Holland T. J. B. (1988) An internally consistent dataset with uncertainties and
632 correlations: 3. Applications to geobarometry, worked examples and a computer program. *J.*
633 *Metamorph. Geol*. **62**, 173–204.

634 Ragone S. E., Datta R. K., Roy D. M. and Tuttle O. F. (1966) The System Potassium Carbonate—
635 Magnesium Carbonate. *J. Phys. Chem.* **70,** 3360-3361. DOI: 10.1021/j100882a515

636 Roest D. L., Ballone P., Bedeaux D. and Kjelstrup S. (2017) Molecular dynamics simulations of
637 metal/molten alkali carbonate interfaces. *J. Chem. Phys. C.* **121**, 17827-17847.

638 Roy R. (1950) Magnesium in fourfold coordination in glass. *J. Am. Chem. Soc.***72**, 3307-3308

639 Sharma, S. K. and Simons B. (1980) Raman study of K_2CO_3-$MgCO_3$ glasses. Carnegie Institute.
640 **79**, 322-326.

641 Shimoda K., Nemoto T. and Saito K. (2008) Local structure of magnesium in silicate glasses: a
642 ^{25}Mg 3QMAS NMR study. *J. Phys. Chem. B* **112**, 6747–6752.

643 Solomatova N.V., Caracas, R. and Manning, C.E. (2019) Carbon sequestration during core
644 formation implied by complex carbon polymerization. *Nat. Commun.* **10**, 789.

645 Staudigel H., Hart S. R., Schmincke H. U. and Smith B. M. (1989) Cretaceous ocean crust at DSDP
646 Sites 417 and 418: Carbon uptake from weathering versus loss by magmatic outgassing.
647 *Geochim. Cosmochim. Acta* **53**, 3091–3094.

648 Thompson R., Smith P., Gibson S., Mattey D. and Dickin A. (2002) Ankerite carbonatite from
649 Swartbooisdrif, Namibia: the first evidence for magmatic ferrocarbonatite. *Contrib. to*
650 *Mineral. Petrol.* **143**, 377–396.

651 Trcera N., Cabaret D., Rossano S., Farges F., Flank A. M. and Lagarde P. (2009) Experimental
652 and theoretical study of the structural environment of magnesium in minerals and silicate
653 glasses using X-ray absorption near-edge structure. *Phys. Chem. Miner.* **36**, 241–257.

654 Vuilleumier R., Seitsonen A., Sator N. and Guillot B. (2014) Structure, equation of state and
655 transport properties of molten calcium carbonate ($CaCO_3$) by atomistic simulations. *Geochim.*
656 *Cosmochim. Acta* **141**, 547–566.

657 Waseda, Y. and Toguri, J.M. (1977) The structure of molten binary silicate systems CaO-SiO_2 and
658 MgO-SiO_2 *Metall. Mater. Trans. B* **8**, 563–568. https://doi.org/10.1007/BF02669331

Table 1. The thermodynamic properties of $MgCO_3$ liquid as derived from the simulations. These are fitted parameters of both a 3rd and 4th order Birch-Murnaghan EOS (Eqs. A1-A4) that have been fitted to the simulations of $MgCO_3$ liquid from 773 to 2000 K up to 20 GPa by the least squares method. $V_{Tr,0}$ is the molar volume at 1100 K and 1 bar; α is the thermal expansion; $K_{Tr,0}$ is the bulk modulus at 1 bar and 1100 K and $\delta K_0/\delta T$ is its temperature dependence; *K'* and *K''* are first- and second-pressure derivatives of the bulk modulus. The root mean square of the pressure residuals of the 4th order fit is 0.06 GPa and of the volume residuals is 0.27 cm^3/mol.

Property	Best Fit (1σ)	
	3rd order EOS	**4th order EOS**
RMS Press. residual (GPa)	0.11	**0.06**
$V_{Tr,0}$ (cm^3/mol)	46.0(2)	**44.21(9)**
α ($10^{-4} \cdot K^{-1}$)	0.004(13)	**1.07(14)**
$K_{Tr,0}$ (GPa)	0.9(20)	**6.15(15)**
$\delta K_0/\delta T$ (10^{-3} · GPa/K)	-0.1(18)	**-1.37(35)**
K'	33(75)	**2.41(1)**
K"		**3.16(1)**

667 **Table 2.** Simulated densities of (Ca, Mg)CO_3 binary liquids approximating compositions of
668 carbonatite melts from phase equilibrium experiments of carbonated mantle (Dalton and Wood
669 1993, Dalton and Presnall 1998, Hammouda 2003, and Ghosh et al. 2009). The pressures and
670 temperatures of the simulations reflect those of the phase equilibrium experiments. Corrected
671 density adjusts the simulated density to account for small concentrations of $FeCO_3$ and SiO_2
672 present in the liquid produced in the original phase equilibrium experiments.

$MgCO_3$ (mol%)	Press. (GPa)	Temp. (K)	Gram formula wt.	Sim.Vol. (cm^3/mol)	Sim. ρ (g/cm^3)	Corrected ρ (g/cm^3)
Dalton and Wood (1993)						
13.6	1.5	1423	98.22	39.19	2.506	2.507
17.4	1.5	1423	97.69	39.23	2.490	2.497
22.5	2.2	1523	96.95	38.28	2.532	2.545
28.7	2.5	1523	96.05	37.76	2.544	2.558
31.6	2.8	1573	95.63	37.47	2.552	2.573
35.1	3.0	1573	95.11	37.09	2.564	2.585
Dalton and Presnall (1998)						
40.9	3.0	1518	93.64	36.59	2.559	2.561
44.0	3.5	1543	93.15	35.94	2.592	2.592
45.8	4.0	1563	92.86	35.44	2.620	2.618
49.2	5.0	1603	92.33	34.54	2.673	2.669
50.9	6.0	1653	92.05	33.77	2.726	2.717
55.5	7.0	1703	91.33	33.03	2.765	2.756
Hammouda (2003)						
10.5	6.0	1523	98.43	34.91	2.820	2.871
10.9	7.0	1273	98.36	33.61	2.927	2.957
10.8	10.0	1373	98.38	32.23	3.052	3.086
14.1	10.0	1473	97.86	32.47	3.014	3.068
Ghosh et al (2009)						
87.1	12.5	1873	86.35	29.53	2.925	3.071
86.8	13.5	1823	86.40	29.12	2.967	3.096
61.1	15.0	1873	90.45	29.62	3.053	3.133
76.1	17.5	1833	88.08	28.30	3.112	3.182

673

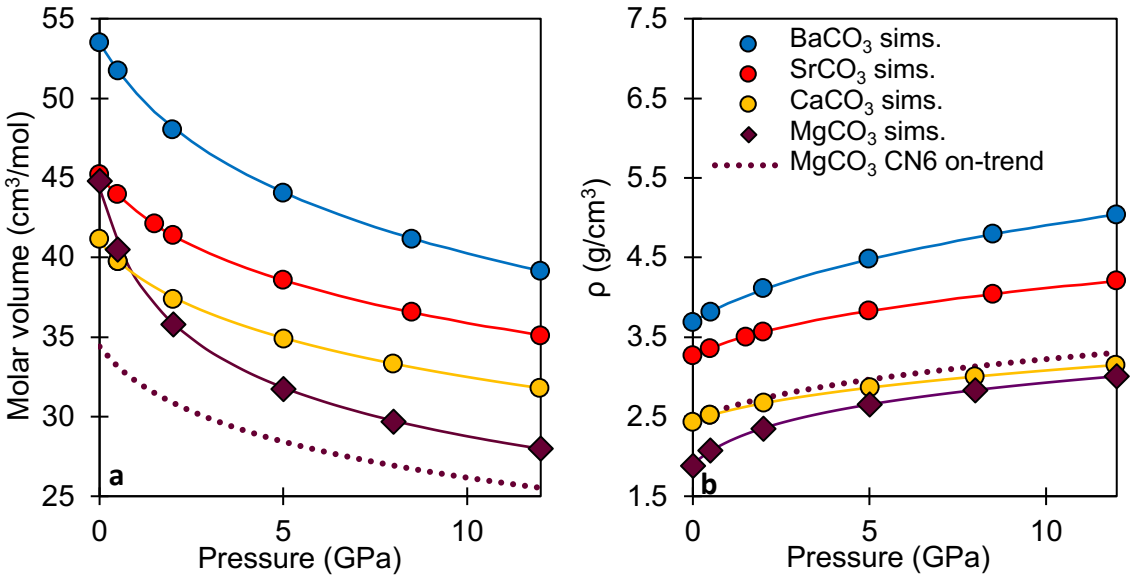

Figure 1. Compression curve of $MgCO_3$ liquid strongly deviates from expectations based on the other alkaline-earth carbonates. Panel a shows simulated molar volumes at 1100 K as a function of pressure for $MgCO_3$, $CaCO_3$, $SrCO_3$ and $BaCO_3$ liquids. Points show simulation results, while solid lines represent best-fit Birch-Murnaghan EOS for each liquid (3rd order for $CaCO_3$, $SrCO_3$ and $BaCO_3$ and 4th order for $MgCO_3$). The dotted line represents the expected compression curve of $MgCO_3$ if its volumetric properties were in-line with periodic trends observed among the other alkaline earth carbonates (i.e. if Mg-C coordination was 6-fold rather than 4). As evident, $CaCO_3$, $SrCO_3$ and $BaCO_3$ form nearly parallel curves that increase systematically from Ca to Ba, while $MgCO_3$ liquid deviates dramatically, especially at low pressure. Panel b shows the same compression curves in terms of density.

674

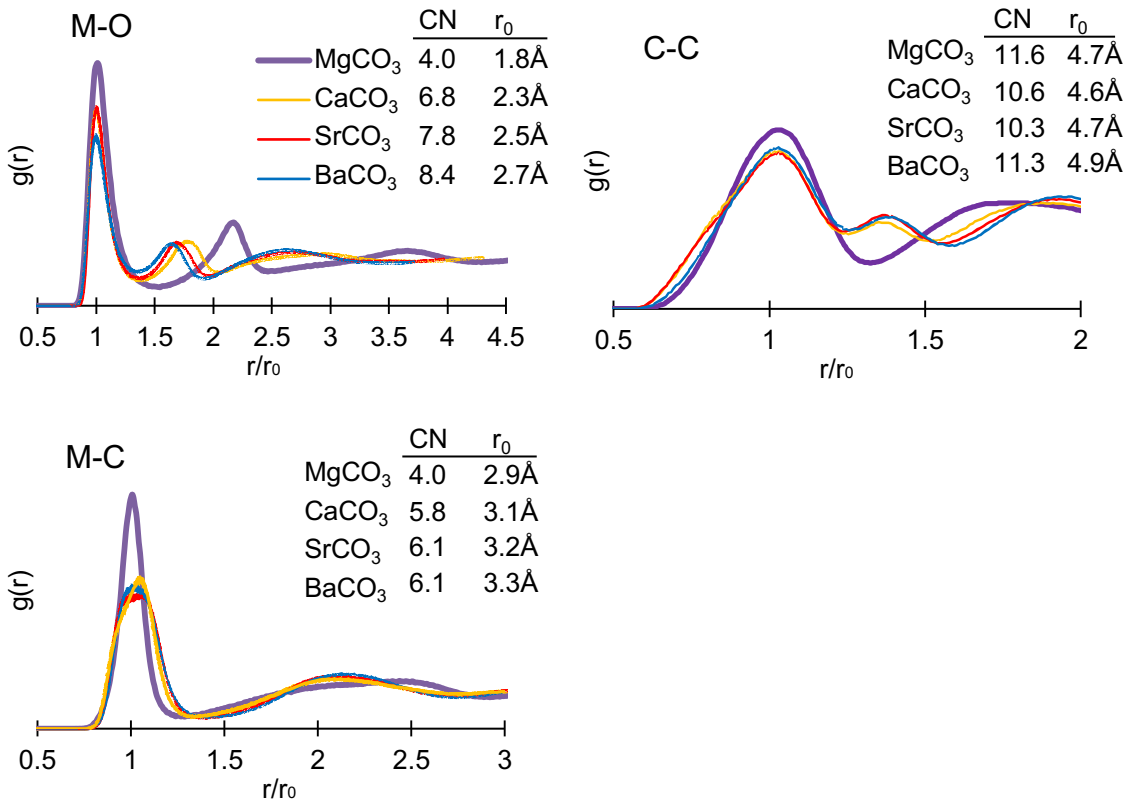

Figure 2. Liquid structure of $MgCO_3$ is distinct from $CaCO_3$, $SrCO_3$ and $BaCO_3$. Pair distribution functions are calculated from liquid simulations at 1 bar and 1100 K for atomic pairs between carbon (C), oxygen (O) and metal cations (M: Mg, Ca, Sr, Ba). The M-O, C-C and M-C pairs shown in panels a, b and c, respectively. For visual comparison, interatomic separation distance (r) has been normalized to the position of the first peak (r_0). Average coordination number (CN) has been calculated for each pair in the embedded tables.

675

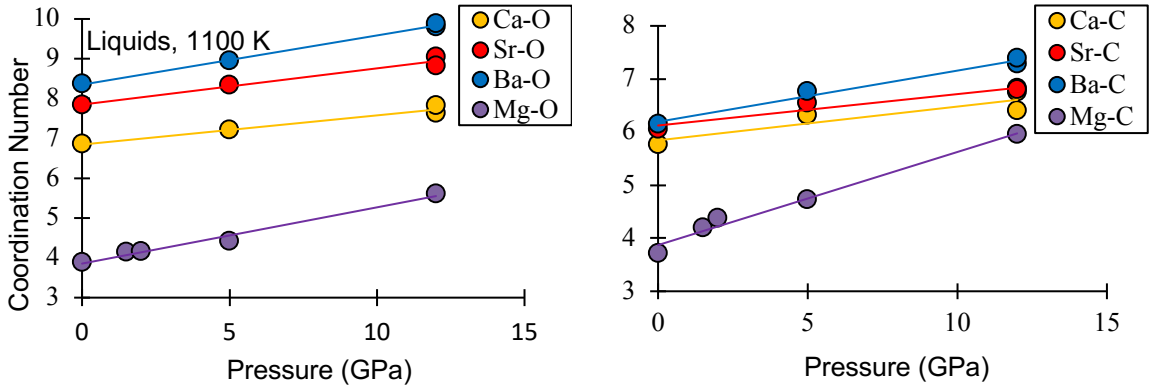

Figure 3. The structure of $MgCO_3$ liquid becomes progressively more like (Ca, Sr, Ba)CO_3 liquids at high pressure. The simulated evolution of coordination for M-O and M-C pairs (in panels a and b), is shown for pure $MgCO_3$, $CaCO_3$, $SrCO_3$ and $BaCO_3$ liquids as a function of pressure up to 12 GPa. In $MgCO_3$, the coordination of M-O and M-C pairs starts at 4 at 1 bar and approaches ~6 at 12 GPa (while other alkaline earths' coordination evolution is more modest, rising 2-4 times slower).

676

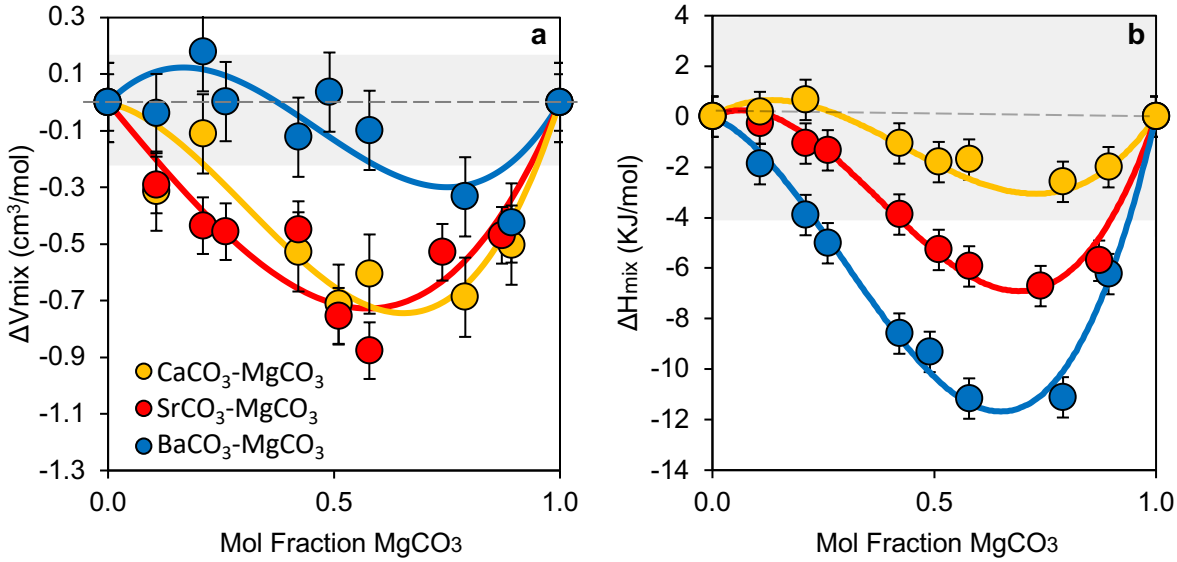

Figure 4. Non-ideal mixing dominates volumetric and enthalpic properties in $MgCO_3$-bearing systems at 1 bar. The ΔV_{mix} (a) and ΔH_{mix} (b) of $MgCO_3$-bearing binary liquids at 1100 K and 1 bar are shown, with non-zero values indicating non-ideal mixing. The shaded regions reflect the range of ΔV_{mix} and ΔH_{mix} for the ideal mixing of (Ca, Sr, Ba)CO_3 liquids calculated by Hurt and Wolf (2018). Both ΔV_{mix} and ΔH_{mix} are, for the most part, negative and reach a minimum at $MgCO_3$ molar concentrations of 0.6 to 0.8. Points show simulation results and lines are the best-fit sub-regular solutions (Eq. 3). Note that, for ΔH_{mix}, simulated total energy values are used instead of enthalpy because they are equal at 1 bar and because simulated total energy has smaller errors than enthalpy due to random fluctuations in both pressure and volume.

678

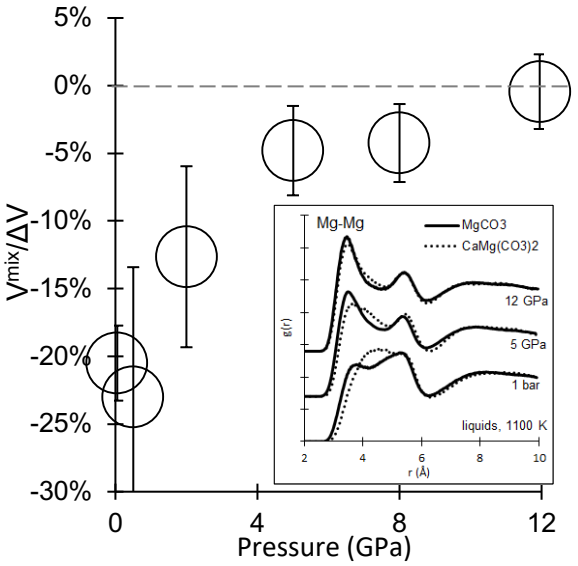

Figure 5. Mixing of molar volumes for $CaCO_3$ and $MgCO_3$ liquid approach ideality with increasing pressure due to a progressively diminishing cation ordering effect. V_{mix} is shown as a function of pressure normalized to $\Delta V_{Ca\text{-}Mg}$ (which is the difference between pure $CaCO_3$ and $MgCO_3$ liquid at the given pressure). As pressure increase, the magnitude of non-ideality approaches 0. The figure inset shows corresponding liquid Mg-Mg pdf curves of pure $MgCO_3$ (solid lines) and $CaMg(CO_3)_2$ (dotted lines) at 1 bar, 2 and 12 GPa. The disparity between the two curves reflects the degree of cation ordering in the liquid. As pressure increase, the mixed $CaMg(CO_3)_2$ curve conforms to that of pure $MgCO_3$.

679

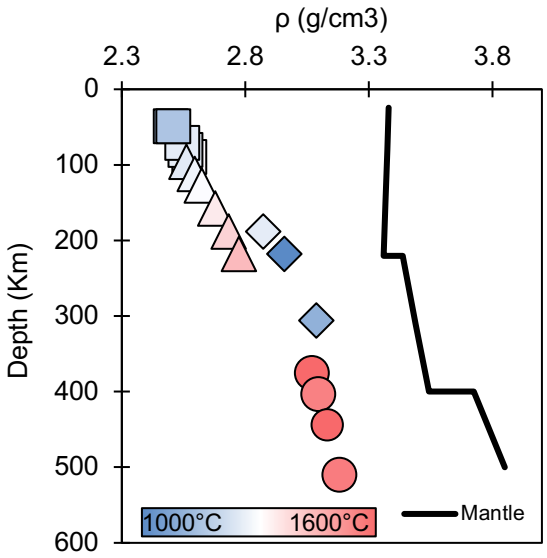

Figure 6. The densities of primary carbonatite melts maintain a high negative density contrast with the surrounding mantle. The simulated densities of $MgCO_3$-$CaCO_3$ binary liquids representing primary carbonatite melts are corrected for minor $FeCO_3$ and SiO_2 concentration and are shown as a function of depth. The simulation temperatures, pressures and compositions are based on the phase equilibrium experiments of Dalton and Wood (1993) (squares), Dalton and Presnall (1998) (triangles), Hammouda (2003) (diamonds) and Ghosh et al. (2009) (circles). Coloring reflects simulation temperature. Mantle density as a function of depth is taken from PREM (Dziewonski and Anderson, 1981).

680

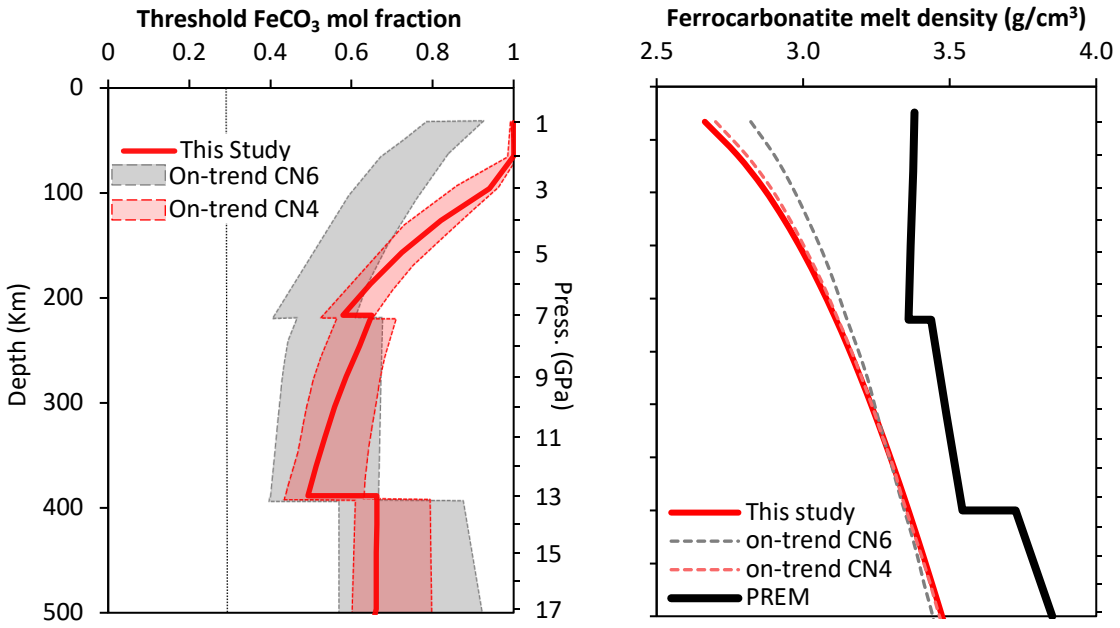

Figure 7. Panel a shows the threshold mole percent $FeCO_3$ necessary for a hypothetical ferrocarbonatite (with composition (Fe_x, $Mg_{0.5\cdot(1-x)}$, $Ca_{0.5\cdot(1-x)}$)CO_3) to achieve neutral buoyancy in the mantle as a function of depth. Three different estimates are depicted: the red line shows results from this study while the gray- and red-shaded regions represent estimated volumetric properties from Hurt (2018), which assume that both Mg^{2+} and Fe^{2+} are in 6-fold and 4-fold coordination with carbonate respectively. The dotted vertical dotted line shows the iron concentration of the only natural, unambiguously-magmatic ferrocarbonatite found in the literature (Thompson et al. 2002). Panel b shows the estimated densities of this natural ferrocarbonatite composition ($Fe_{0.26}$ $Mg_{0.22}$ $Ca_{0.52}$ CO_3) calculated for the three models (red lines are simulations from this study and the optimal on-trend CN6 and CN4 models from Hurt 2018 are shown in gray- and red-dashed lines) along with the density of PREM (Dziewonski and Anderson, 1981).

681

Appendices

A. Equations of state used to model simulation data

The simulated molar volumes of $MgCO_3$ liquid were used to fit the parameters of the EOS below (adapted from Angel 2000):

$$P = 3K_{T,0}f_E(1+2f_E)^{\frac{5}{2}}\{1 + c3\, f_E + c4\, f_E^2\} \quad \text{Eq. A. 1}$$

$$c3 = \frac{3}{2}(K' - 4)\,, \quad c4 = \frac{3}{2}\left[K_{T,0}K'' + (K' - 4)(K' - 3) + \frac{35}{9}\right]$$

where $K_{T,0}$ is the isothermal bulk modulus at 1 bar and simulation temperature (T), c3 and c4 are the 3rd and 4th order EOS terms, which are written in terms of the fitted parameters K' and K'' (the 1st and 2nd pressure-derivatives of the bulk modulus). $K_{T,0}$ is a function of temperature according to:

$$K_{T,0}(T) = K_{Tr,0} + \frac{\delta K_0}{\delta T}(T - 1100\ K) \quad \text{Eq. A. 2}$$

$(\frac{\delta K_0}{\delta T})$ is the fitted 1bar temperature dependence of the bulk modulus and $K_{T,0}$ is the fitted 1 bar bulk modulus at the reference temperature. The Eulerian finite strain, f_E, is defined as:

$$f_E = \left[\left({V_{T,0}}/{V_{T,P}}\right)^{2/3} - 1\right]/2 \quad \text{Eq. A. 3}$$

$V_{T,P}$ is the simulation volume at T and pressure (P). $V_{T,0}$ is the volume at 1 bar and T and can be calculated from the fitted 1 bar volume at 1100 K ($V_{Tr,0}$) and the fitted thermal expansion (α). $V_{T,0}$ thus becomes:

$$V_{T,0} = V_{Tr,0}e^{\alpha(T - 1100\ K)} \quad \text{Eq. A. 4}$$

The parameter α is the fitted 1 bar thermal expansion coefficient, assumed to be temperature-independent.

B. Comparison of $MgCO_3$ to alkali carbonate liquids

MD simulations of $MgCO_3$ liquid indicate that, at ambient pressure (where $MgCO_3$ liquid is unstable) Mg^{2+} assumes a 4-fold coordination with both the carbonate molecule and oxygen much like alkali carbonate liquids, Li_2CO_3, $NaCO_3$ and K_2CO_3 (e.g. Roest et al. 2017; Kohara et al. 1999). This stands in stark contrast to $CaCO_3$-$SrCO_3$-$BaCO_3$ liquids in which metal cations are in 6-fold coordination with carbonate and 7- to 8-fold coordination with oxygen (Hurt and Wolf 2018). The similarity between $MgCO_3$ and alkali carbonate liquid structure is well-illustrated by a comparison of pdf curves for $MgCO_3$ liquid versus Li_2CO_3 liquid, as shown in Figure B.1 (Roest et al. 2017). This resemblance in liquid structure (and

physical properties) is not unprecedented; it's partially explained by the Mg-Li diagonal relationship, in which the compounds of certain elemental pairs (Li-Mg, Be-Al, B-Si and C-P) that are diagonally adjacent on the Periodic Table, share some properties in common. Thus, it's expected that liquid $MgCO_3$ volumetric properties should be similar to that of Li_2CO_3.

Alkali carbonates generally have a larger volume than their alkaline earth counterparts, not only because of the additional metal cation per formula unit but because the partial molar volume of $(CO_3)^{2-}$ is greater, ~38 cm^3/mol versus 31 cm^3/mol (Hurt and Lange 2019). The partial molar volume of $(CO_3)^{2-}$ is greater in alkaline earth carbonate liquids because of changes in network topology, not because the size of the carbonate molecule actually increases (See Hurt and Lange 2019 for a full discussion).

C. Structure and thermodynamics of $MgCO_3$-carbonate mixtures

C.1 Pdf curves of $MgCO_3$ mixtures

Pdf curves showing the liquid structures are shown for all pure endmember melts as well as 50:50 mixtures along each $MgCO_3$-bearing binary in Figure C.1. To better understand the liquid structure with respect to carbon-carbon pairs, the pdfs of $MgCO_3$, $CaCO_3$, and $CaMg(CO_3)_2$ liquid are shown in Figure C.2, along with a theoretical weighted average of the endmembers. Figure C.3 shows distributions of various coordination numbers for M-O and M-C pairs for a selection of compositions at different temperatures and pressures.

C.2 Structural ordering and non-ideality in $MgCO_3$ mixtures

The thermodynamic and structural properties of $MgCO_3$-bearing liquids are explored through molecular dynamic simulations. The conditions and basic results for each run are summarized in Table C.1, including simulations of pure $MgCO_3$ as well as binary mixtures of $MgCO_3$ with $CaCO_3$, $SrCO_3$ and $BaCO_3$ liquids. The detailed results of binary mixtures and associated excess properties are reported in Table C.2, and the best-fit asymmetric sub-regular solution model parameters are presented in Table C.3.

As noted above, liquid properties (e.g. molar volume, compressibility, enthalpy and heat capacity) do not mix ideally in the $MgCO_3$-binary compositions as they do in the $CaCO_3$-$SrCO_3$-$BaCO_3$ liquid system at 1 bar. The non-ideal source of this mixing should likely manifest as some structural anomaly evident in the pdf curves of mixtures (i.e. there should be some noticeable difference between the pdf curves of pure $MgCO_3$ compared to an $MgCO_3$-bearing mixture). Such a difference might help reveal the mechanism driving non-ideal mixing behavior.

Simulations reveal that the key structural difference between pure and mixed $MgCO_3$ liquids is metal cation ordering. In pure $MgCO_3$ liquid at 1 bar, the primary Mg-Mg coordination shell is actually composed of two partially overlapping shells. The inner shell contains 3 Mg atoms at an average distance of 3.7 Å, and the outer shell has an additional 9 Mg atoms at an average distance of 5.3 Å. When $MgCO_3$ is mixed with another carbonate, this primary coordination shell is split, with the inner shell preferentially filled by other metal cations. Figure C.4 shows the Mg-Mg and Mg-Ca pdf curves in pure $MgCO_3$ and $MgCa(CO_3)_2$; these curves show that Mg^{2+} vacates the inner coordination shell in mixed compounds and is replaced by Ca^{2+}. This kind of cation ordering was not observed in $CaCO_3$-$SrCO_3$-$BaCO_3$ liquids. Such ordering in $MgCO_3$-bearing mixtures can explain why some properties of $MgCO_3$-bearing liquids do not mix ideally, while $CaCO_3$-$SrCO_3$-$BaCO_3$ liquids do. This behavior is likely related to cation ordering in the calcite-dolomite-magnesite series, which produces the highly ordered dolomite structure, where cations of mixed sizes are accommodated with minimal lattice strain (Vinograd 2006). Given that V_{mix} is found to be either negative or insignificant, cation ordering likely allows the liquid to pack space more efficiently for liquid Mg-carbonate mixtures.

D. Description of density simulation corrections

The simulation results presented in the main text highlight the novel topology of $MgCO_3$ liquid and provide estimates of its thermodynamic properties and mixing behavior which is important for future integration of the $MgCO_3$ liquid component into thermodynamic modeling software such as MELTS or THERMOCALC. However, the pair potential model can also be directly applied to geologic systems by providing property estimates of natural carbonatite liquids at relevant temperatures and pressures. In order to estimate the density of primary carbonatite melts generated by low-degree partial melting of carbonated mantle, simulations are performed in the $CaCO_3$-$MgCO_3$ liquid system. The simulated liquid compositions, temperatures and pressures are based on the results of phase equilibrium experiments carbonated mantle partial melting experiments.

To constrain the composition of carbonatite melts produced by partial melting of the carbonated mantle, Dalton and Wood (1993) and Dalton and Presnall (1998) conducted phase equilibrium experiments on carbonated peridotite systems at pressures ranging from 1.5 to 7 GPa and temperatures from 1423 to 1703 K. Hammouda (2003) and Ghosh et al. (2009) conducted similar experiments for carbonated eclogite in the 6-17.5 GPa pressure range. They produced carbonate melts with > 92 wt. % $CaCO_3$ and $MgCO_3$ for the peridotite-derived melts and > 88 wt. % for the eclogite-derived. The remaining wt. % is mostly $FeCO_3$ and SiO_2. We estimate the densities of the primary carbonate melts of Dalton and Wood (1993), Dalton and Presnall (1998), Hammouda (2003) and Ghosh et al. (2009) by simplifying them to $CaCO_3$-$MgCO_3$ binary

compositions and simulating them at their respective temperature and pressure conditions. The simulated $CaCO_3$-$MgCO_3$ melts range in density between 2.49 to 3.11 g/cm^3 at 1.5 and 17.5 GPa respectively; the full results are presented in Table 2. Since the minor $FeCO_3$ and SiO_2 components are omitted in these simulations, the raw simulated densities have been corrected to account for their absence.

An approximate correction to the simulated densities may be made by assuming $FeCO_3$ has the same partial molar volume as the $MgCO_3$ melt component and integrating it into the density calculation. The density may be further corrected by accounting for the SiO_2 liquid component of the carbonatite melt by using the volumetric data from Lange and Carmichael (1987) and Kress et al. (1988) and assuming the SiO_2 volume mixes ideally into the carbonate melt. Table 2 gives the simulated melt composition, gram formula weight, molar volume and simulated density along with the $FeCO_3$-SiO_2-corrected density.

E. M-O bond length evolution with pressure

Figure E.1 below shows the evolution of metal cation-oxygen (M-O) bond lengths as a function of pressure for at 1100 K. While M-O bond length in $CaCO_3$, $SrCO_3$ and $BaCO_3$ decrease with pressure as expected, $MgCO_3$ actually *increases*. This paradoxical behavior is analogous to the well-known observed properties for a variety of silicate liquids (including pure silica, MORB, basalt, and enstatite), which also shows a compression-induced bond-length increase for Si-O up to ~40 GPa (Karki et al. 2018). Similarly, bond-length expansion is likewise seen in Al-O up to ~20 GPa. In every one of these cases, we see a cation in a low coordination state with oxygen near ~4 at ambient pressure. Pressure is thus accommodated primarily in every case by increasing coordination evolution, which readily outweighs the countervailing effect of bond length extension. Given the apparent universality of this behavior for coordination evolution at the low end of the spectrum, we thus focus our discussion primarily on the changes in overall liquid structure connected to changes in the Mg-C and Mg-O coordination.

F. High-temperature (2000 K) compression curves $MgCO_3$ and $CaCO_3$ liquid

Figure F.1 below shows the evolution of metal cation-oxygen (M-O) bond lengths as a function of pressure for at 1100 K. While M-O bond length in $CaCO_3$, $SrCO_3$ and $BaCO_3$ decrease with pressure as expected, $MgCO_3$ actually *increases*. This paradoxical behavior is analogous to the well-known observed properties for a variety of silicate liquids (including pure silica, MORB, basalt, and enstatite), which also shows a compression-induced bond-length increase for Si-O up to ~40 GPa (Karki et al. 2018). Similarly, bond-length expansion is likewise seen in Al-O up to ~20 GPa. In every one of these cases, we see a cation in a low coordination state with oxygen near ~4 at ambient pressure.

118 Pressure is thus accommodated primarily in every case by increasing coordination evolution, which
119 readily outweighs the countervailing effect of bond length extension. Given the apparent universality of
120 this behavior for coordination evolution at the low end of the spectrum, we thus focus our discussion in this
121 manuscript primarily on the changes in overall liquid structure connected to changes in the Mg-C and Mg-
122 O coordination.

123 **Appendix References**

124 Kohara S. (1999) A reverse Monte Carlo study of molten lithium carbonate. *Plasmas & Ions* **83**, 79–83.

125 Kress V. C., Williams Q. and Carmichael I. S. E. (1988) Ultrasonic investigation of melts in the system
126 Na_2O-Al_2O_3-SiO_2. *Geochim. Cosmochim. Acta* **52**, 283–293.

127 Lange R. A. and Carmichael I. S. E. (1987) Densities of Na_2O-K_2O-CaO-MgO-FeO-Fe_2O_3-Al_2O_3-TiO_2-
128 SiO_2 liquids: New measurements and derived partial molar properties. *Geochim. Cosmochim. Acta*
129 **51**, 2931–2946.

130 Vinograd V. L., Winkler B., Putnis A., Gale J. D. and Sluiter M. H. F. (2006) Static lattice energy
131 calculations of mixing and ordering enthalpy in binary carbonate solid solutions. *Chem. Geol.* **225**,
132 304–313.

133

Table C.1. The complete simulation results are shown below. Total energy and Enthalpy are relative to their respective values for $MgCO_3$ at 1100 K and 0 GPa. 1 σ error on temperature is 2 K, 0.02 GPa for pressure, 0.1 cm^3/mol for volume, 0.2 KJ for total energy and 0.9 KJ for enthalpy.

	Temp. (K)	Press. (GPa)	Mol. Vol. (cm^3/mol)	Tot. Energy (KJ/mol)	Enthalpy (KJ/mol)
			Pure $MgCO_3$		
	773	0.00	43.10	-49	-49
	1100	0.00	44.48	0	0
	1499	0.00	46.46	61	61
	2000	0.00	47.98	136	136
	1099	0.49	40.52	-2	17
	900	1.99	35.39	-32	-
	1101	2.01	35.84	-2	70
	1500	2.02	36.85	58	132
	1869	2.98	35.89	112	219
	2273	3.58	35.97	170	299
	1101	4.99	31.74	2	160
	1101	5.00	31.74	3	161
	1501	5.00	32.66	61	224
	1100	8.00	29.71	8	245
	2274	8.05	31.96	173	430
	1099	12.01	28.03	17	353
	1500	11.99	28.67	72	416
	1099	15.01	27.14	25	432
	2000	14.95	28.41	147	571
	1100	19.99	26.07	39	560
Mol frac. $MgCO_3$		***$CaCO_3$-$MgCO_3$ Simulations***			
0.11	1100	0.00	41.06	196	195
0.12	1424	1.49	39.19	239	298
0.14	1424	1.49	39.28	236	294
0.15	1423	1.54	39.23	232	291
0.15	1372	9.98	32.23	223	544
0.17	1423	1.46	39.14	227	284
0.2	1523	2.21	38.28	235	319
0.21	1099	0.00	43.06	43	43
0.21	1101	0.00	41.62	174	173
0.22	1523	2.20	38.35	230	314
0.22	1523	2.20	38.35	230	314
0.26	1523	2.49	37.76	222	316
0.28	1573	2.83	37.47	224	329
0.29	1525	2.52	37.70	216	310
0.32	1573	2.84	37.33	217	322
0.32	1572	3.03	37.09	216	328
0.35	1518	2.98	36.71	200	309
0.35	1573	3.01	36.99	208	319
0.35	1572	3.01	36.88	208	318
0.4	1544	3.50	36.12	191	317
0.41	1519	2.98	36.59	187	296

0.42	1100	-0.01	41.94	126	125
0.44	1543	3.50	35.94	184	309
0.46	1563	4.00	35.44	183	324
0.51	1100	-0.01	42.06	105	104
0.51	1100	-0.01	42.06	105	104
0.51	1998	0.01	46.60	249	249
0.51	1100	0.50	40.05	104	124
0.51	1100	2.00	36.41	102	174
0.51	1799	2.98	37.15	207	317
0.51	1800	2.99	37.16	207	318
0.51	1573	4.98	34.42	176	347
0.51	1099	4.99	33.13	103	268
0.51	1603	5.02	34.54	181	354
0.51	1655	5.98	33.77	184	386
0.51	1100	8.00	31.33	108	358
0.51	1100	12.00	29.86	117	475
0.56	1703	7.03	33.03	183	414
0.58	1102	0.00	42.41	91	90
0.61	1873	14.97	29.62	205	648
0.76	1834	17.48	28.30	174	668
0.79	1099	0.00	43.06	43	43
0.87	1873	12.48	29.53	150	518
0.87	1821	13.54	29.12	145	538
$SrCO_3$-$MgCO_3$ Simulations					
0.11	1100	0.01	44.89	291	291
0.21	1100	0.00	44.66	257	256
0.26	1101	-0.01	44.60	240	239
0.42	1099	0.01	44.48	185	185
0.49	1100	11.99	31.51	172	549
0.51	1100	0.00	44.11	154	154
0.51	2000	0.03	48.71	299	300
0.58	1100	-0.01	43.93	131	131
0.74	1100	0.01	44.15	78	78
0.87	1100	0.00	44.11	36	36
$BaCO_3$-$MgCO_3$ Simulations					
0.11	1100	0.00	52.52	422	421
0.26	1101	0.00	51.18	346	346
0.42	1099	0.01	49.59	266	266
0.49	2000	-0.02	53.57	373	372
0.49	1099	12.00	33.60	247	650
0.58	1100	0.00	48.19	189	188
0.79	1099	0.00	46.04	89	88
0.89	1100	0.01	45.02	45	45

137

138

Table C.2: The volume and enthalpy results of MgCO3-bearing binary simulations at 1100 K and 1 bar are shown below. Ideal volumes and enthalpies and ΔV_{mix} *and* ΔH_{mix} calculated according to Eq. 7 and 8 are also listed.

Comp. Mol%$MgCO_3$	Mol. Vol. (cm^3/mol)	Ideal Vol. (cm^3/mol)	ΔV_{mix} (cm^3/mol)	Enthalpy (KJ/mol)	Ideal H (KJ/mol)	ΔH_{mix} (KJ/mol)
			$CaCO_3$-$MgCO_3$			
0.0	41.00	41.00	0.00	218.9	218.9	0.0
10.7	41.06	41.37	-0.31	195.7	195.5	0.2
21.0	41.62	41.73	-0.11	173.6	173.0	0.7
42.1	41.94	42.47	-0.53	125.6	126.7	-1.1
51.0	42.06	42.78	-0.71	105.4	107.2	-1.8
57.9	42.41	43.01	-0.61	90.5	92.2	-1.7
79.0	43.06	43.75	-0.69	43.4	46.0	-2.6
89.3	43.60	44.11	-0.50	21.5	23.5	-2.0
100.0	44.48	44.48	0.00	0.0	0.0	0.0
			$SrCO_3$-$MgCO_3$			
0.0	45.26	45.26	0.00	326.0	326.0	0.0
10.7	44.89	45.18	-0.29	290.8	291.1	-0.3
21.0	44.66	45.10	-0.44	256.5	257.6	-1.1
26.0	44.60	45.06	-0.46	239.9	241.2	-1.3
42.1	44.48	44.93	-0.45	184.8	188.7	-3.9
51.0	44.11	44.86	-0.76	154.4	159.7	-5.3
57.9	43.93	44.81	-0.88	131.4	137.3	-5.9
74.0	44.15	44.68	-0.53	78.1	84.8	-6.7
87.2	44.11	44.58	-0.47	36.1	41.8	-5.7
100.0	44.48	44.48	0.00	0.0	0.0	0.0
			$BaCO_3$-$MgCO_3$			
0.0	53.53	53.53	0.00	475.0	475.0	0.0
10.7	52.52	52.56	-0.04	422.2	424.1	-1.9
21.0	51.81	51.63	0.18	371.4	375.3	-3.9
26.0	51.18	51.17	0.00	346.4	351.4	-5.0
42.1	49.59	49.71	-0.12	266.3	274.9	-8.6
49.0	49.13	49.09	0.04	233.0	242.3	-9.3
57.9	48.19	48.29	-0.10	188.9	200.1	-11.2
79.0	46.04	46.38	-0.33	88.6	99.7	-11.1
89.3	45.02	45.45	-0.43	44.7	50.9	-6.2
100.0	44.48	44.48	0.00	0.0	0.0	0.0

Table C.3: Gives the coefficients fitted to Eq. 1 to describe both ΔV_{mix} and ΔH_{mix} calculated by our simulations of liquids in each of the three binaries at 1100 K and 1 bar.

	ΔV_{mix} (cm^3/mol)		ΔH_{mix} (KJ/mol)	
	w	Δw	w	Δw
$CaCO_3$-$MgCO_3$	-2.91	-6.78	-7.33	-35.51
$SrCO_3$-$MgCO_3$	-3.625	-3.77	-22.90	-62.56
$BaCO_3$-$MgCO_3$	-1.345	-6.47	-40.20	-92.95

Figure B.1. The liquid structure of $MgCO_3$ is similar to that of Li_2CO_3. The liquid pdf curves of $MgCO_3$ from our simulations (solid lines) are compared to those of Li_2CO_3 generated by FPMD simulations from Roest et al. 2017 (dotted lines) at 1200 K and 15 kbar. $CaCO_3$ liquid at 1200 K and 15 kbar is shown for comparison (grey dashed line). $MgCO_3$ liquid is more like Li_2CO_3 than $CaCO_3$.

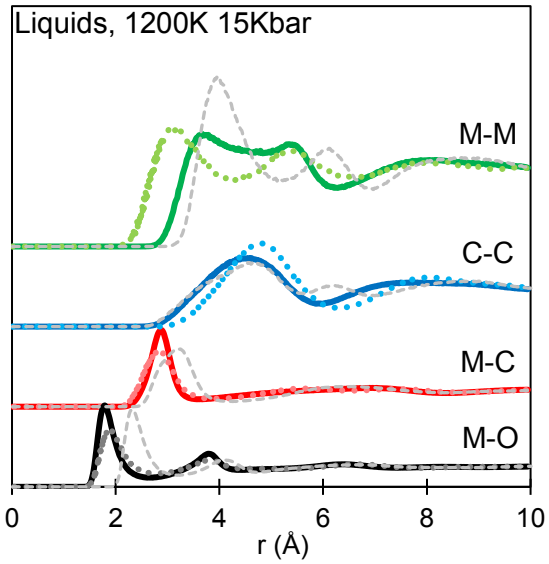

Figure C.1: PDF curves for M-O, C-C and M-C pairs in pure liquids are unchanged by mixing. The coordination of M^{2+} with oxygen atoms and carbonate groups is unaffected by the composition of the liquid. The carbon-carbon pdf curve changes when Mg^{2+} is introduced into the mix but remains a weighted average of the two endmember components (Appendix. 4).

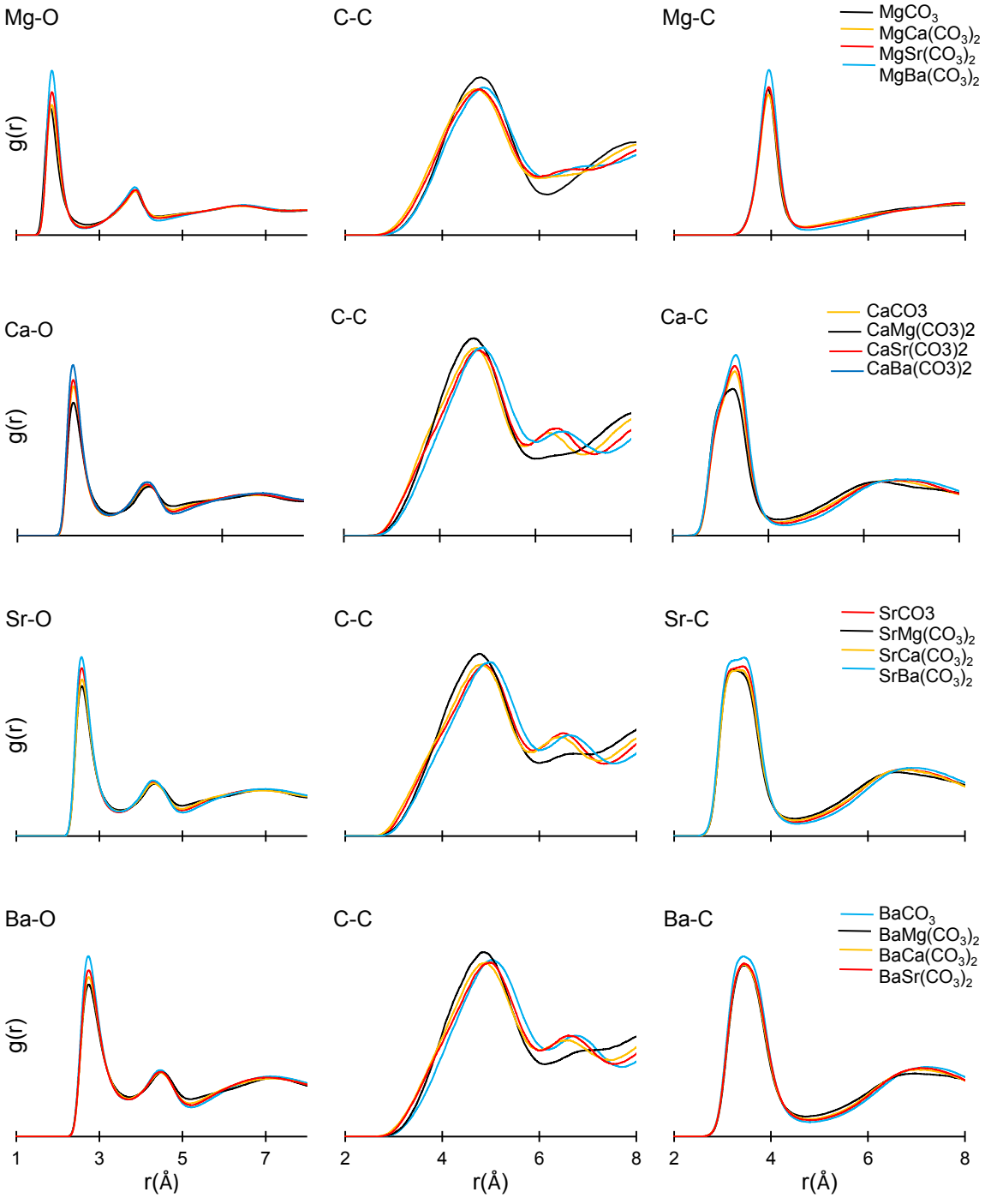

Figure C.2: Structural packing of carbonate molecules varies systematically for Mg-bearing carbonate mixtures. Shown below are pdf curves from simulations of C-C pairs (at 1100 K and 0 bar) for pure $MgCO_3$ liquid (purple line), pure $CaCO_3$ (yellow line) liquid and an intermediate binary composition, $CaMg(CO_3)_2$ (orange line). The black line is the C-C pdf curve of $CaMg(CO_3)_2$ calculated from the composition-weighted average of the two end members which nearly perfectly predicts the simulated structure; this demonstrates that carbonate packing is not responsible for deviations from ideality in $CaCO_3$-$MgCO_3$ mixtures.

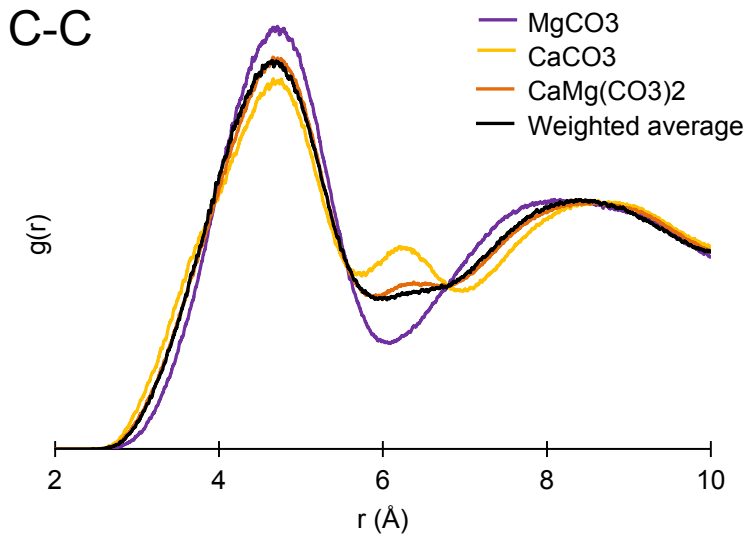

Fig. C.3: Coordination number histograms for M-O and M-C pairs. The distribution of various coordination number states of M-O and M-C pairs are shown at a variety of temperatures and pressures for a selection of various compositions.

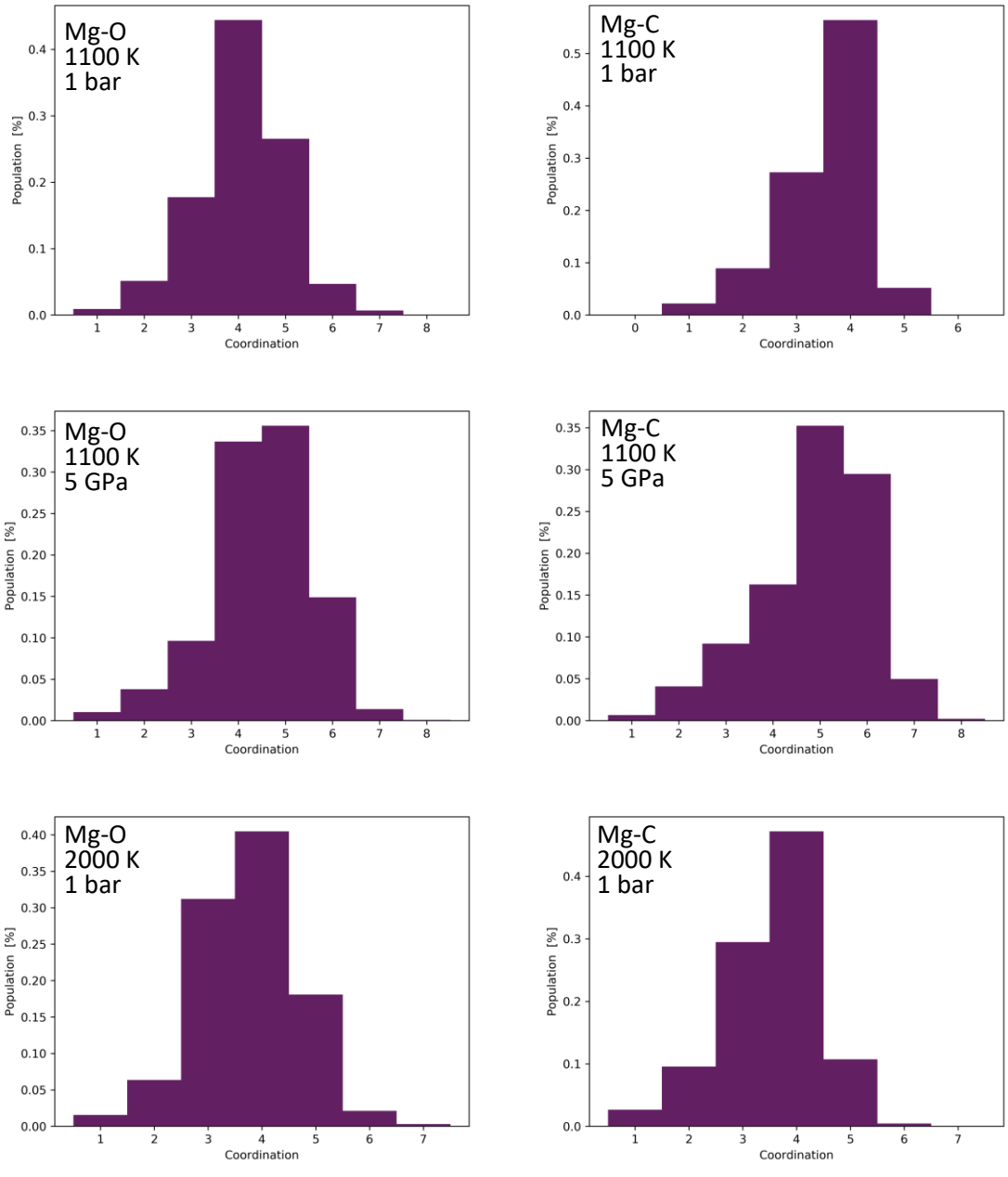

194

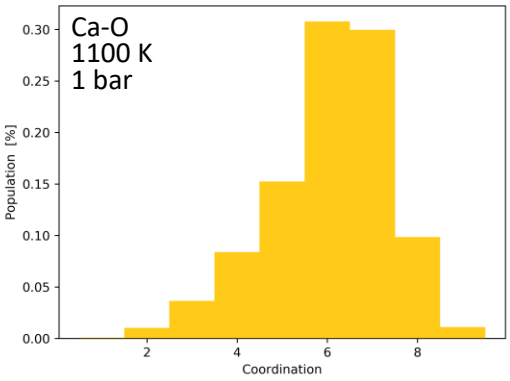

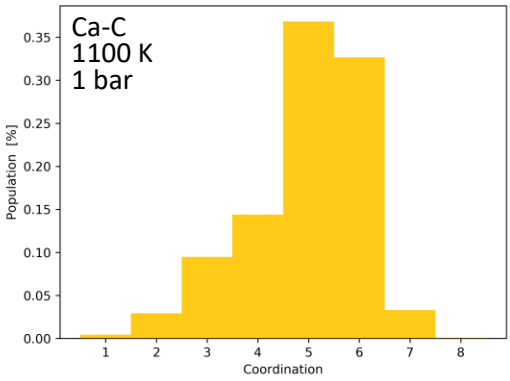

195

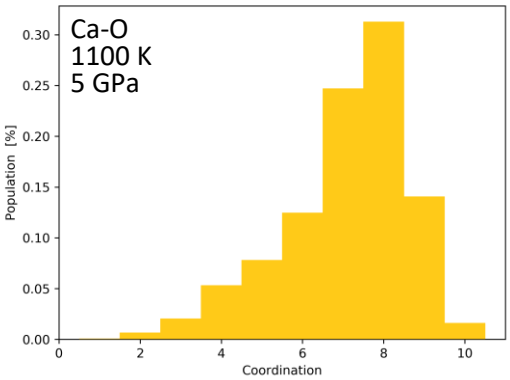

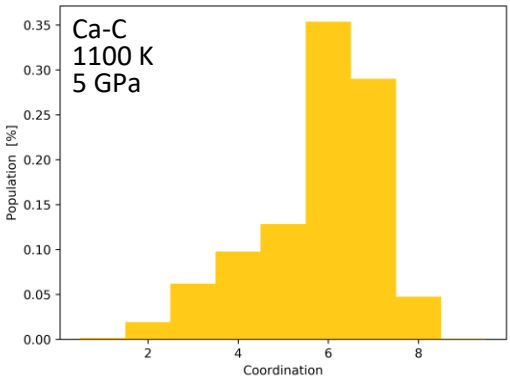

196

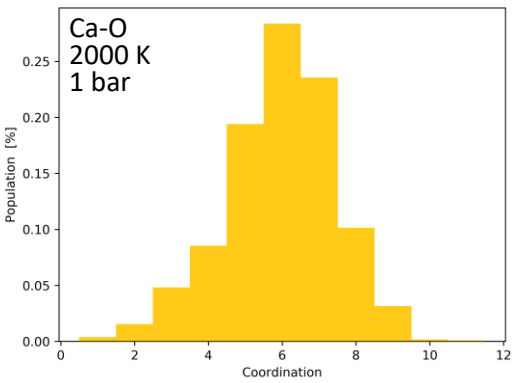

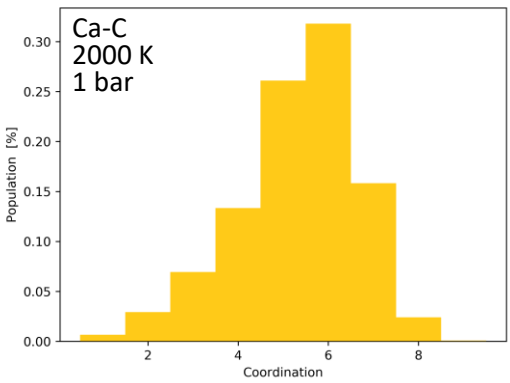

197

198

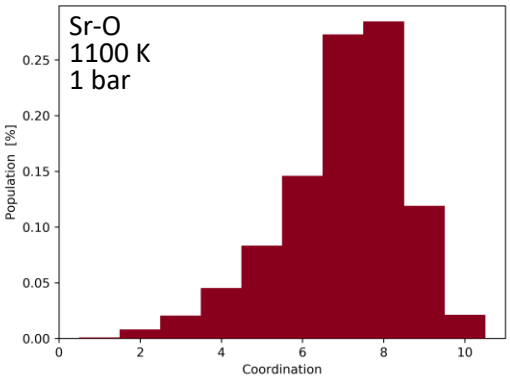

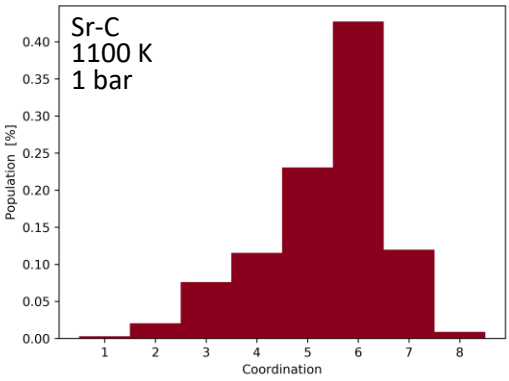

199

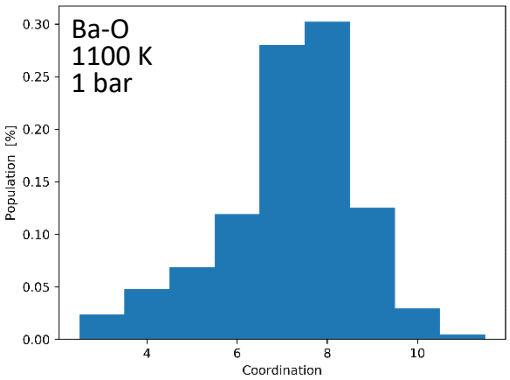

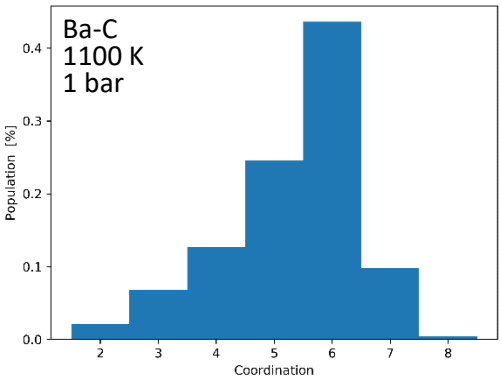

200

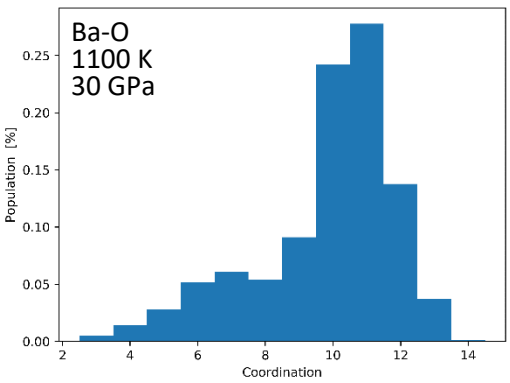

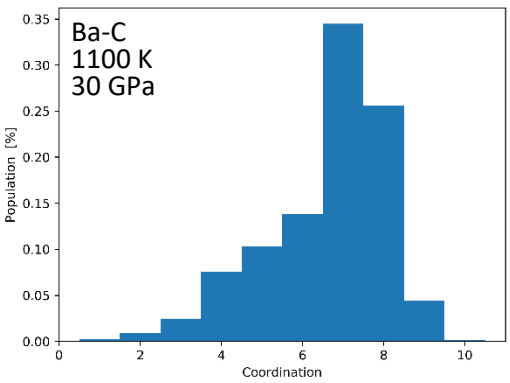

201

202

203

204

205

Figure C.4. Mg-Mg pdf curve in pure $MgCO_3$ liquid are significantly altered upon mixing due to Mg^{2+} vacating the inner coordination shell in favor of Ca^{2+}, Sr^{2+} or Ba^{2+} ions. The pdf curves are generated from simulations of pure $MgCO_3$ liquid and a mixture, $CaMg(CO_3)_2$, at 1100 K and 1 bar. The inner coordination shell (CN=3) in pure $MgCO_3$ disappears in the mixture and is filled with Ca^{2+}. This same effect occurs in $MgCO_3$ mixtures with the other alkaline earth cations (Sr^{2+} and Ba^{2+}). This likely results from an energetic penalty for Mg^{2+} to be surrounded by other Mg^{2+} ions; the preferential ordering observed here results from surrounding the Mg-CO_3 tetrahedral complexes with the $(Ca, Sr, Ba)^{2+}$ octahedral complexes, and might be favored as a mechanism to handle cation size mismatch that relaxes stresses in the atomic structure.

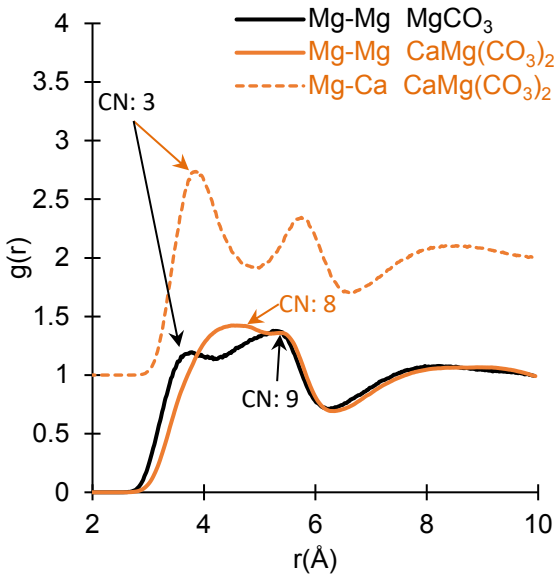

Figure E.1. Cation-oxygen bond-length evolution occurs alongside coordination evolution. As shown, all other alkaline earth carbonate liquids show standard bond-length compression with increasing pressure, while Mg-O bonds show paradoxical bond-length expansion, mirroring Si-O expansion in many silicate liquids.

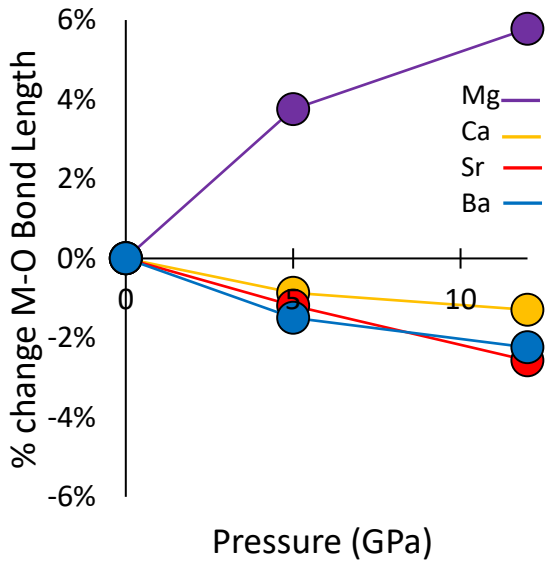

Figure F.1. Compression curves for Mg and Ca carbonate liquid at high temperature (2000 K). We find strong agreement with the lower temperature results at 1100 K (see Fig 1 of manuscript), where the hypothetical compression curve—assuming 6-fold coordination for Mg—represents the high-pressure limiting behavior as the liquid structure of $MgCO_3$ evolves toward that of the other alkaline earth carbonates.